UNIVERSITY OF OKLAHOMA

GRADUATE COLLEGE

RESERVOIR QUALITY EVALUATION OF THE MERAMEC AND UPPER OSAGE UNITS IN THE ANADARKO BASIN

A THESIS

SUBMITTED TO THE GRADUATE FACULTY

in partial fulfillment of the requirements for the

Degree of

MASTER OF SCIENCE

By

JEFFREY HARDWICK
Norman, Oklahoma
2018

RESERVOIR QUALITY EVALUATION OF THE MERAMEC AND UPPER OSAGE UNITS IN THE ANADARKO BASIN

A THESIS APPROVED FOR THE
CONOCOPHILLIPS SCHOOL OF GEOLOGY AND GEOPHYSICS

BY

Dr. R. Douglas Elmore, Chair

Dr. Shannon Dulin

Dr. Zulfiquar Reza

ACKNOWLEDGEMENTS

First, I would like to thank Dr. Elmore for the opportunity to join his research group at OU. His constant guidance and direction throughout this project were instrumental to the quality of work produced. I would also like to thank Dr. Shannon Dulin and Zulfiquar Reza for the insight each of you provided in the review and discussion of my thesis. Thank you to Devon Energy for the data provided in this study, as well as Katie Garrett, Jason Currie, David Hull, and Tom Peryam for facilitating the project that significantly added to my professional development. I would also like to thank my friends and colleagues that have contributed to my work in various fashions, including: Gerhard Heij, Cory Terrell, Matt Hamilton, Christina Hamilton, and the numerous undergraduates that have worked long hours in the paleomagnetism lab. Lastly, I would like to thank my family, specifically, my dad and grandfather for the constant drive and support to reach my goals.

Table of Contents

LIST OF FIGURES

ABSTRACT

The objective of this study is to provide a comparative look at the diagenetic evolution and reservoir quality characteristics of the Meramec and Upper Osage units in the STACK (Sooner Trend Anadarko Basin of Canadian and Kingfisher counties) and NW STACK (extension of the STACK, to the northwest, into portions of Dewey, Blaine, Woodward, and Major counties, Oklahoma). Both are hybrid unconventional plays in the Anadarko Basin of Oklahoma and consists of a complex depositional sequence of Middle Mississippian siliciclastics and carbonates of Meramecian and Osagean age as well as the Late Devonian to Early Mississippian organic-rich Woodford Shale.

Unsupervised Hierarchical Clustering Analysis (HRA) was performed to connect reservoir-scale petrophysical observations with micro-scale petrographic observations. The clustering analysis yielded five distinct electrofacies in the Meramec that represent depositional trends in mineralogy and diagenetically enhanced intervals of anomalous feldspar dissolution. Implementing HRA provided a genetic-based workflow for reservoir quality prediction and understanding. Wireline data from twelve publicly available wells with core and wireline data from seven other wells provided the framework to demonstrate the predictive workflow presented in this study.

Paleomagnetic and petrographic data were integrated to discern the diagenetic evolution of each unit. Petrographic analysis revealed a pervasive marine calcite cement in silt-dominated microfacies of the Osage and Meramec. The calcite cement significantly occluded primary porosity and created baffles for vertical fluid flow. The terrigenous input of clay partially protected primary porosity enhancing fluid flow in the more framework dominated microfacies. The primary pore-types observed in good reservoir quality

microfacies include: intragranular pores in feldspars, interstitial porosity in clay, and intergranular pores in between other framework grains such as silt. Thermal demagnetization revealed a characteristic remanent magnetization (ChRM) removed at unblocking temperatures ranging from 250°C to 450°C. The ChRM displayed shallow inclinations consistent with an acquisition of approximately 300 Ma. The ChRM is interpreted as a chemical remanent magnetization (CRM) related to the emplacement of hydrocarbons; thus, providing a critical temporal component on the evolution of the petroleum system.

INTRODUCTION

The integration of advanced drilling and completion designs have revolutionized our ability to extract hydrocarbons from unconventional oil and gas reservoirs. While much attention has been placed on developing primary self-sourced shale reservoirs, hybrid tight oil and gas reservoirs are proving economically viable under the appropriate geologic conditions and commodity prices. The STACK (**S**ooner **T**rend **A**nadarko Basin of **C**anadian and **K**ingfisher counties (Miller, 2018)) is one such hybrid play in the Anadarko Basin of Oklahoma. The STACK is comprised of a complex depositional sequence of Middle Mississippian siliciclastics and carbonates of Meramecian (Meramec-Unit) and Osagean (Osage-Unit) age as well as the underlying Late Devonian to Early Mississippian Woodford Shale (Price, 2017). The Woodford Shale acts a vital source rock in the Anadarko Basin (Johnson et al., 1992) and the overlying Meramec and Osage units are low permeability reservoirs that likely rely on charging from the Woodford Shale to be economically producible.

Of the many criteria involved in the migration and subsequent charging of reservoirs by hydrocarbons; the evolution of the pore system is one that requires diligent characterization. Diagenetic processes such as cementation, illitization, and albitization are a few of the processes that can have a strong influence on the dynamic evolution of a pore system (Morad, 2010). Diagenesis encompasses any process from deposition to metamorphism (Ali et al., 2010). Conventional wisdom from Hayes (1979) provides four key fundamentals on diagenetic interactions in sandstones. They are: primary intergranular porosity and associated permeability are significantly reduced during burial due to compaction, cementation, and a number of other mechanisms; secondary porosity can be

created at depth from the dissolution of unstable framework grains; chemical processes are kinetically controlled and the pore fluid acts as the operating medium; and finally, the given path of a lithotype from source to sink presets the diagenetic reactions during progressive burial. These fundamental concepts of sandstone diagenesis are most viable in a principally siliciclastic depositional environment. Mixed siliciclastic-carbonate sequences can comprise a much different style of diagenesis because calcite is hundreds of times more soluble than quartz in near-surface conditions (Ali, 2010). Therefore, a number of modifications can occur that are associated with the mobilization of calcite into the pore fluid. In a shallow marine setting, seawater is the initial fluid in primary pore space. This can result in the precipitation of marine carbonate cements occluding a significant volume of the initial porosity (Ali, 2010). In a mixed siliciclastic-carbonate depositional setting both sediment types can be cemented by marine seawater because each may have sufficient primary porosity to accommodate flow near the sediment water interface (Morad, 2010).

This project aims to investigate the diagenesis and reservoir quality of one such mixed siliciclastic-carbonate sequence defined by the Meramec and Upper Osage units in the STACK and NW STACK (**N**orth **W**est extension of STACK). The study area covers portions of Woodward, Dewey, Major, Blaine, Canadian, and Kingfisher counties in Oklahoma, as outlined in Figure 1. The project contributes to the understanding of how micro-scale textural fabrics (diagenetic and depositional) relate to storage and flow property variations while also adding insight into the diagenetic evolution of the Meramec and Osage. These contributions were accomplished through the integration of petrography, petrophysics and paleomagnetism utilizing seven cores and twelve publicly available wells. The principal goals of this study were to:

1. Identify the diagenetic or depositional control on reservoir quality.
2. Connect micro-scale observations to reservoir-scale observations.
3. Devise a petrophysical workflow for predicting reservoir quality.
4. Define the paragenesis of the Meramec and Osage.
5. Test for a secondary magnetization that may date diagenetic events.

Achieving these goals will prove the hypothesis that the reservoir quality of the mixed siliciclastic-carbonate depositional sequence of the Meramec and Osage is strongly connected to depositional facies. It will also allow for the integration of micro-scale and reservoir-scale observations creating a genetic petrophysical workflow for reservoir quality prediction and understanding. A second hypothesis to test is that the Meramec and Osage were diagenetically influenced by hydrothermal fluids and contain a chemical remanent magnetization (CRM) as a result.

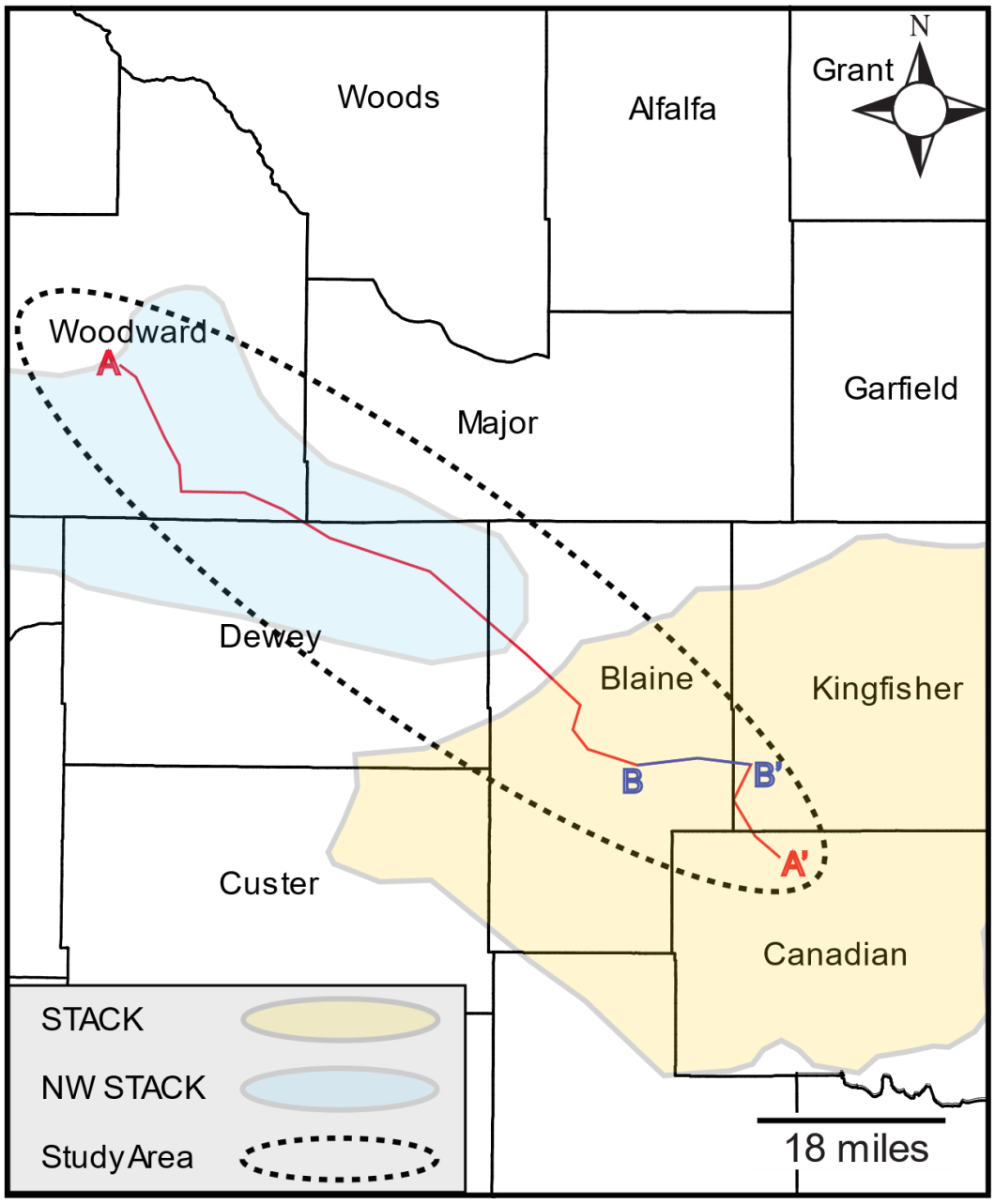

Figure 1: Base map showing the outline of the study area with the STACK play in yellow (modified from Cullen, 2017), and the NW STACK inferred from IHS Enerdeq (October 2018). The red solid line from A to A' defines the transect for the cross section in Figure 7 and B to B' defines the transect for Figure 9.

GEOLOGIC SETTING AND PREVIOUS WORK

The study area for the Meramec and Osage is situated on the northeastern margin of the Anadarko Basin (Figure 2). The Meramec and Osage sediments were deposited in the predecessor Oklahoma Basin, which was the regional depocenter that defined the paleo-bathymetry throughout Osagean and Meramecian time (Johnson, et al., 1989). The Oklahoma Basin covered a large portion of the Southern Midcontinent, extending from Oklahoma to Arkansas and smaller portions of Kansas, Colorado, and Texas (Johnson et al., 1989). It developed in response to broad subsidence and epeirogenic movements acting on the lithosphere during the Late Cambrian though Mississippian, similar to a passive margin, as referred to by Nicholas and Rozendal (1975); and Keller et al. (1983). Johnson et al. (1989) described the basin as having a shelf geometry with a significant volume of marine deposits that thicken into proto-basins such as the Anadarko Basin. Within the Oklahoma Basin, the Southern Oklahoma Aulacogen acted as the primary depocenter (Ham and Wilson, 1967; Gilbert, 1983). The aulacogen is the site of the failed arm of a continental rift from the Cambrian (Wickham, 1978). Extensive magmatic overprinting of the upper lithosphere and the subsequent cooling phase initiated the subsidence that provided the accommodation space for the aulacogen to act as the primary depocenter in the Oklahoma Basin (Feinstein, 1981; Carter et al., 1998; Keller, 2014).

The Anadarko Basin (see Figure 2) is referred to by Perry (1989) as the deepest sedimentary basin within the North American continent. It is bounded to the east by the Nemaha Uplift, to the south by the Wichita Uplift, and to the west by the Cimarron Arch (Johnson et al., 1989). In the southern portions of the basin, near the margin with the Wichita Uplift, Paleozoic sedimentary strata can be as thick as 40,000 feet (12,000 meters). The

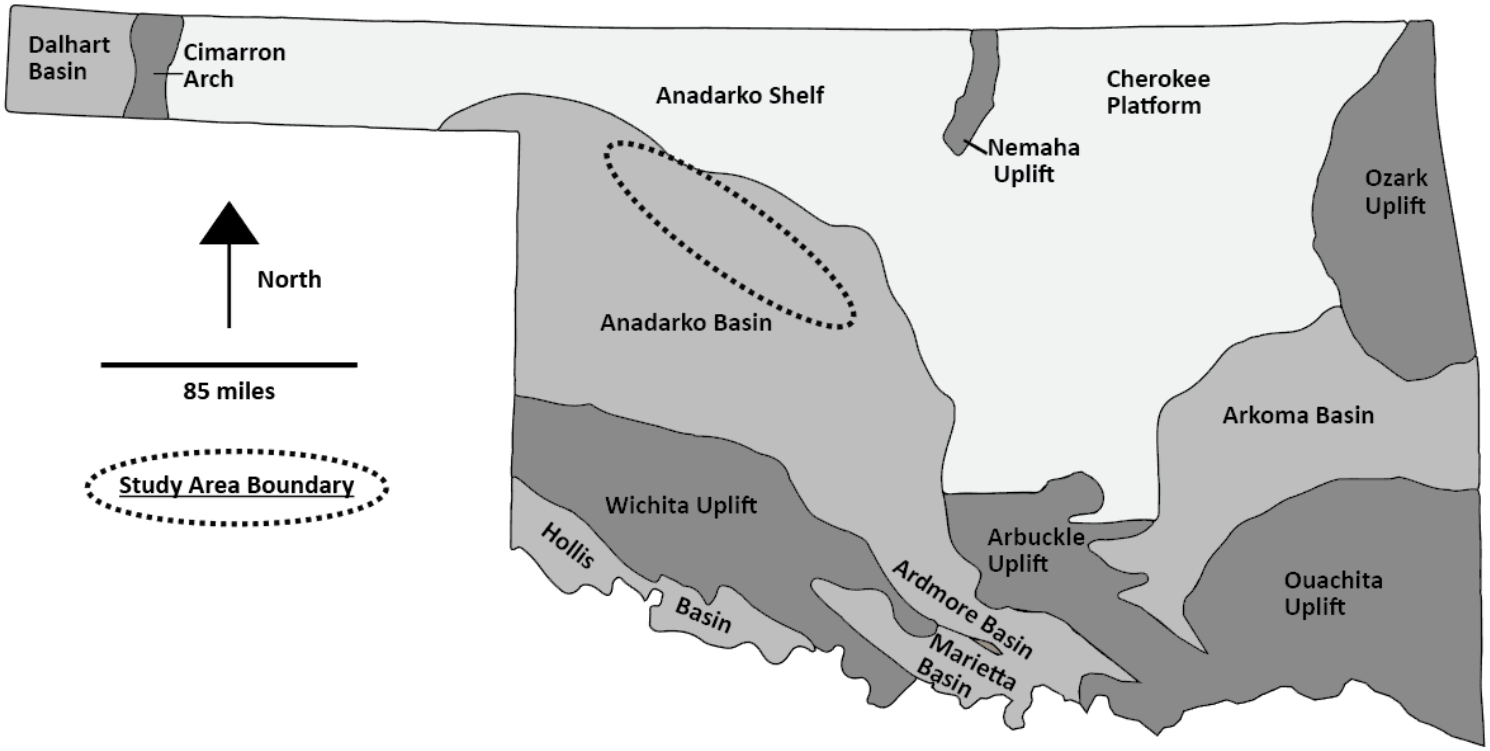

Figure 2: Geologic provinces within the state of Oklahoma. The study area is outlined by the dashed oval and the geologic provinces such as a basin or uplift are outlined by a black line. Modified from Northcutt and Campbell (1998).

northern reaches of the basin, nearing the shelf, exhibit significant asymmetry resulting in a much thinner package of sedimentary strata nearing 10,000 feet (3,000 meters) (Johnson et al., 1989).

Through much of the Early and Middle Paleozoic the Anadarko Basin and adjacent Wichita-Amarillo crustal blocks were coupled and gently subsided in the Oklahoma Basin. Late Morrowan time punctuated the most rapid subsidence due to a collisional event between the North American and Gondwanan lithospheric plates, referred to as the Ouachita orogeny (Johnson et al., 1989; Perry, 1989). The orogeny inverted the Cambrian rift providing a structural boundary for the Anadarko Basin. It also uplifted and detached the Wichita-Amarillo block from the Anadarko block nearly 40,000 feet (12,000 meters) along regional reverse faults (Johnson et al., 1989).

Within the study area, the Meramec is underlain by variably thick intervals of Osage carbonates and Upper Devonian to Early Mississippian Woodford Shale (Figure 3). Overlying the Meramec is Chesterian associated strata of the Chester Shale and Springer Group (Figure 3). The Meramec and Osage within the study area do not have a biostratigraphic constraint, rather each are defined by their unique log characteristics (Figure 3) and correlations between the STACK and NW STACK. The top of the Meramec is defined by an abrupt decrease in resistivity and increase in gamma ray associated with the increased clay content of the Chester Shale. The top of the Osage (or base of Meramec) is generally defined by a sudden increase in resistivity and decrease in gamma ray due to tight carbonates in the section. Locally, within the NW STACK, the resistivity may be lower and more variable at this boundary because of lenticular or brecciated diagenetically altered chert.

Previous studies of Osagean and Meramecian associated strata have focused primarily

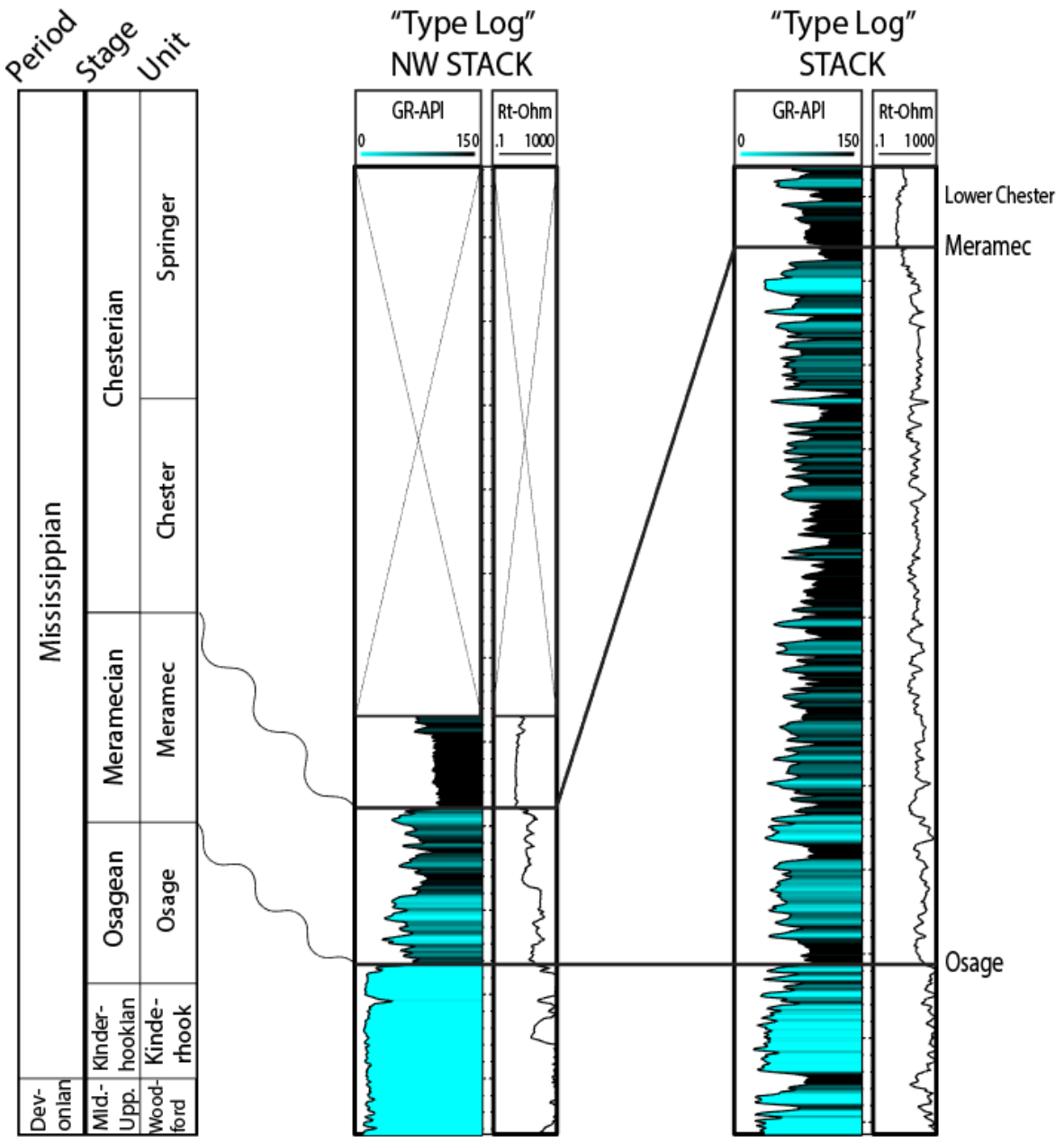

Figure 3: (Left Track) – Stratigraphic nomenclature for the study area (modified from Boyd, 2008). (Middle and Right Track) – Type logs the NW STACK and STACK illustrating the top of the Meramec, Osage and the lower portion of the Chester interval with gamma ray (left track) and deep resistivity wireline logs (right track). The NW STACK type log is from Dewey county and the STACK type log is from Canadian county.

on the up-dip Mississippi lime formation and down-dip Sycamore formation. The Mississippi lime formation is a mix of carbonates and cherty carbonates that are prolific hydrocarbon reservoirs through the mid-continent of the U. S. (Wethington, 2017). Many of the studies (Mikkelson, 1966; Parham and Northcutt, 1993; Rogers, 1996; Watney, 2001; Rogers, 2001) have investigated the depositional and diagenetic origin of anomalous reservoir properties in the Mississippi "Chat". Rogers (2001) reported the chat as eroded or weathered detritus of the Mississippi lime from topographic highs on the Burlington Shelf in northern Oklahoma and Kansas. The chat is unique in its anomalous pore volume (can exceed 20%) owing to a prime mix of silicification of carbonate detritus and leaching of any remaining calcite in the meteoric realm (Rogers, 2001). More recent studies have investigated specific up-dip equivalent strata such as the division of the Cowley Formation by Mazzullo, (2009). Mazzullo illustrated the Cowley Formation's sequence stratigraphic significance as a transgressive and high-stand systems tract on the edge of the Burlington Shelf.

Numerous studies of the down-dip Sycamore formation in the Arbuckle Mountains have reported the subsurface correlation of the Sycamore formation implementing outcrops as comparative markers (Prestidge, 1957; Braun, 1958; Culp, 1961). Schwartzapfel (1996) identified partial Bouma sequences as well as groove and flute casts in the Sycamore formation in the Arbuckle Mountains. These observations drove their interpretation of the Sycamore formation as representing gravity flows in a deep-water setting. Sycamore deposition by turbidity currents and other gravity flows is still accepted in more modern reports (Coffey, 2000; Miller, 2018).

Until recent, Harris (1975) is one of the few investigations of the Meramec and Osage within the study area. The study reported on the difficulties in interpreting the Meramec from

the Osage in subsurface correlations and described the variations of facies present from silty carbonates to more clay dominated intervals through the section. With the recent increase in operations in the STACK play, a revived interest has developed on revisiting the fundamental understanding of these units. An emphasis has been placed on providing insight into the depositional system and sequence stratigraphic hierarchy. A series of retrogradational and progradational parasequence sets defined by northeast-southwest strike-elongate clinoforms have been identified by Price et al. (2017) and Miller (2018). The Meramec has been proposed by Price et al. (2017) to represent strata influenced by basinal currents in a subaqueous delta setting with deposition below storm-weather wave base. Miller (2018) postulates for deposition on a shallow ramp between fair-weather wave base and just below storm-weather wave base with reworking by storms and basinal currents.

Regional diagenesis work of Meramecian and Osagean correlative strata in northcentral Oklahoma by Dehcheshmehi (2016) found homogenization temperatures greater than 140°C in carbonate and quartz cements which is nearly ~50°C higher (Cardott, 2014) than the burial temperature for the area. Dehcheshmehi (2016) suggested the dispersion of these temperatures may be related to pulses of thermal anomalies from deeper basinal fluids in Ordovician and Cambrian strata. Further postulating, the migration of these fluids may be related to basinal fluid flow activity during the Ouachita and Appalachian orogenies (Dehcheshmehi, 2016). A diagenetic study of the Woodford Shale in the southeastern Anadarko Basin by Roberts (2017) also postulated a relationship between hydrothermal fluids and the Ouachita orogeny. Therefore, the regional paleo-plumbing system that seems to have diagenetically altered Mississippian strata may also influence the diagenesis within the study area.

DATA AND METHODS

Seven vertical, un-oriented cores from the northern margin of the Anadarko Basin were provided by Devon Energy for the study. The data provided with each core is as follows: thin sections at a variable sampling rate of a 1-2 feet, with a total of seven hundred and fifty-six between all cores; triple-combo wireline logs which include gamma ray (GR), deep – resistivity (AT90), neutron porosity (NPHI), and bulk density (RHOB); core gamma ray; x-ray diffraction mineralogical analysis (only in the Meramec); and core photos.

Petrography

Seven hundred and fifty-six thin sections were impregnated with blue epifluorescent epoxy and polished to a thickness of thirty microns. The epoxy helps with the identification of micropores under ultraviolet light that may not protrude completely through the thin section because of their small size or asymmetry. Thin sections were also stained with a mixed concentration of alizarin red and potassium ferricyanide; calcite is stained red, potassium feldspars are stained yellow, and ferroan carbonates or zoned ferroan carbonates are stained blue. Thin section analysis was performed under plane-polarized, cross-polarized, reflected, and ultraviolet light on a Zeiss AxioImager.Z1m. Photomicrographs were captured with a linked AxioVision microscope camera attachment. The analysis focused on organizing each thin section into a microfacies classification scheme, to characterize the regional variability of depositional and/or diagenetic alteration within the study area. The microfacies classification was based on grain size, sorting, volume proportion of primary framework grains to secondary authigenic components, and the common pore – types present. An emphasis was

also placed on determining the interplay of the depositional texture and diagenetic overprint on the evolution of the pore system. Quantitative mineral volume determinations via point counting were not carried out due to the number of thin sections; however, upon the adequate classification of microfacies for a given core, the x-ray diffraction data was used to supplement the microfacies classification scheme. The x-ray diffraction data was integrated after the thin section analysis to avoid bias in the microfacies classification scheme. Core photos provided supplemental observations to confirm thin section observations, but a conventional core description was not utilized in this study for microfacies identification. A core description was not performed because of the densely spaced thin sections made available and the microscale stratigraphic variability that is present in core requiring thin section confirmation.

A FEI Quanta 250 scanning electron microscope (SEM) and Bruker XFlash 6I100 x-ray detector (EDX) were utilized in imaging pore-types across microfacies to provide a supplemental micro-scale in determining pore-sizes and potential overgrowths. The EDX also provided a quantitative means for determining elemental analysis of detrital, authigenic, and other phases unidentifiable or with otherwise ambiguous optical properties. Image segmentation was attempted; however, the polishing of the thin sections did not allow for successful results. SEM analysis was pivotal in confirming the observations made on the petrographic microscope and bridged the rest of the study in comparing the variety of scales integrated in the study to characterize the reservoir quality of the Meramec and Osage.

Petrophysics

Mapping

To establish a framework that provided a regional comparison between the STACK

and NW STACK an effort was placed on adding extra stratigraphic information between each core with publicly available wells. Therefore, approximately one thousand five hundred well logs across Woodward, Major, Dewey, Blaine, Kingfisher, and Canadian counties were acquired from IHS Enerdeq. Mapping and correlation of the Meramec and Osage intervals followed in IHS Petra on the wells that had the intervals present and the log suites that made the picks allowable. The subsurface mapping culminated in a regional stratigraphic comparison through a cross-section from the NW STACK to STACK instead of regional isopachs or reservoir models. Twelve publicly available wells with the accompanying log suites of GR, AT90, DPHI, and NPHI were digitized in Petra's digitizing module to integrate in the cross section. Finally, within the Meramec interval additional internal picks were made based on interpreted flooding surfaces and shallowing depositional sequences.

Hierarchal Clustering Analysis

A principal goal of this study was to make an asserted effort to complement the petrographic work at the micro and nano-scale to a more practical reservoir scale with log responses. To achieve this, unsupervised Hierarchal Clustering Analysis (HRA) was implemented to organize the available log suites into similar responses. The term "electrofacies" is used to describe the output of HRA into clusters of data by well log responses. These clusters are ideally defined by variations in mineralogy, fabric, thickness, and petrophysical properties that potentially relate to diagenetic or depositional processes (AlBahadily and Nasser, 2017).

The inputs to the HRA were GR, AT90, RHOB, and NPHI. For each of the nineteen wells used in the HRA workflow, the GR log was normalized with a cumulative histogram over the Meramec interval. Minimum and maximum percentiles of five and ninety-five,

respectively, transformed the magnitudes within the Meramec of the publicly available wells. RHOB and NPHI were normalized in a similar fashion. The STACK and NW STACK associated well logs were separated during normalization to achieve calibration from geologically similar areas.

Log normalization was followed by numerous clustering runs each with a different number of defined modes. Each mode configuration was projected in principal component space (as in Figure 4) to deem the range of statistically viable mode configurations. The range of mode configurations were also plotted in petrophysical space. This allows the user to consider the practicality of a given mode definition to the goal of clustering itself. Finally, the microfacies of the seven cored wells were plotted next to the electrofacies to compare the representation of the variability observed petrographically to the responses of the well logs. HRA was applied exclusively to the cored wells due to the constraint of the thin sections. Core images with each of these wells also allowed for the consideration of the sampled interval thickness to the corresponding log resolution. The centroids of the final clustering output also detailed the association of the data in the publicly available wells to a specific cluster based on its Euclidian distance. In turn, allowing for the ability to predict the electrofacies defined by the microfacies to the publicly available wells.

Total Porosity and Fluid Saturation Models

To supplement the interpreted storage capacity and hydrocarbon potential for specific intervals in the Meramec models for both total porosity (no core porosity available) and fluid saturation were developed. The total porosity was calculated from cross-plot porosity of NPHI and DPHI. This method incorporates a shale volume (VSHALE) correction. VSHALE was calculated and normalized to clay volume from XRD data throughout the Meramec. Due to

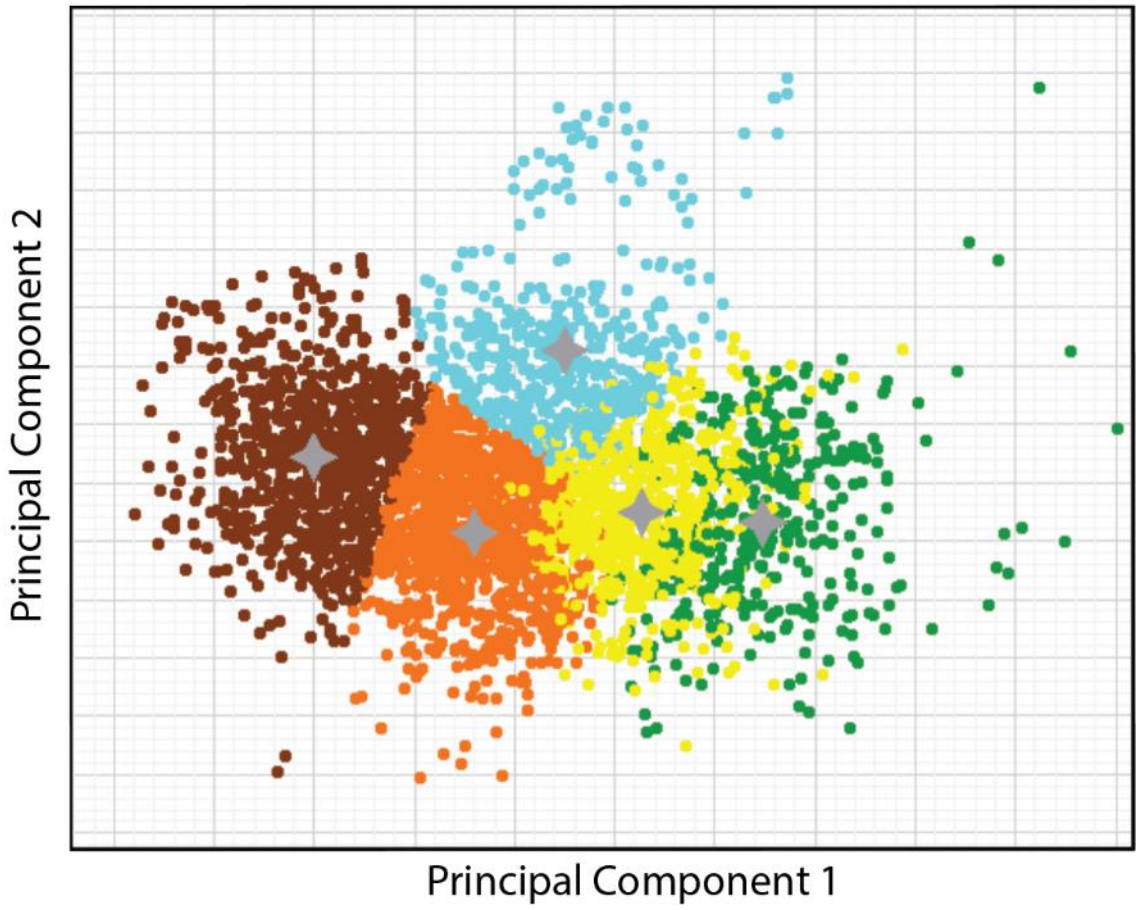

Figure 4: An example of clusters projected along each principal component axis from one of the cored wells

the clay content in the Meramec and concern for overestimated water saturation a dual water saturation method was used that would account for clay distribution with VSHALE as an input. The other inputs to the water saturation model were a formation water resistivity of .05, a cementation exponent of 1.77, and saturation exponent of 1.77 (Puzin, 1951). The purpose of the fluid saturation and total porosity models was to define how each parameter varies though the section. It is quite possible that the magnitudes predicted in each of these models could be quite different than actual reservoir conditions, but the trends should be similar.

Paleomagnetism

Samples from an un-oriented core in Dewey county were collected for the paleomagnetic portion of the study. The samples were oriented relative to a scribe line and cut by a water-cooled drill press at the University of Oklahoma. All samples were cut further into (2.2-centimeter length) specimens to have multiple data points for each stratigraphic sampling interval. Two demagnetization methods were applied: alternating field (AF) and thermal demagnetization. Fifteen specimens were demagnetized by AF in steps of 10 mT up to 120 mT. The remaining sixty-two were thermally demagnetized in steps of 100°C from natural remanent magnetization (NRM) 200°C and 25°C from 200°C to 700°C. At each step the NRM was measured in a 2G Enterprises three-axis cryogenic magnetometer with DC SQUIDS. Analysis of the paleomagnetic data was performed in the SuperIAPD program picking principal components as defined by Krischvink (1980) on plots of the orthogonal projections of inclination and declination (Zijederveld, 1967). Mean angle of deviation (MAD) was below fifteen degrees for each component. Inclination only values were calculated (Aronson and Levy., 2010) and used to determine the age of magnetizations by comparison to expected inclinations for the study area.

RESULTS AND INTERPRETATIONS

To logically organize the observations of the petrography in the Meramec and Osage the two will be subdivided in the following section. The primary microfacies of each unit in the STACK and NW STACK will be defined and the more local secondary microfacies that are diagenetically significant will also be described.

Osage Microfacies

The Osage consists of differing microfacies in the NW STACK as compared to the STACK. The NW STACK is comprised of two primary microfacies: chert and skeletal grainstone (Figure 5). The STACK consists of six primary microfacies, each of which are more diluted by silt than the NW STACK. They are: skeletal packstone, muddy wackestone, siltstone, fossiliferous siltstone, spiculite, and chert (Figure 6).

NW STACK

Chert (Figure 5-A): The chert microfacies is most common in the uppermost part of the section and is observed in forms of lenticular and nodular chert as a replacement of a previous carbonate depositional fabric by microcrystalline silica. Calcite, dolomite and de-dolomite are also authigenic and are locally present throughout. The microcrystalline silica matrix preserves ghost fabrics of the previous allochems through the overall geometry and subtle crystal size variations. These fabrics are most prevalent in sponge spicules along transects and horizontal slices. Locally, dissolution of the silica matrix is present, and the dissolution seems to preferentially dissolve sponge spicules (Figure 5-B). These pores can range from a few microns to twenty microns and can locally exceed ten volume percent pore space. The chert microfacies are often bound by dissolution seams. The seams accumulate

insoluble material such as clay and solid bitumen (Figure 6-C). Bitumen is often present on the outer rim of chert nodules adjacent to dissolution seams (Figure 6-D). The chert also contains vertical fractures filled with authigenic phases such as silica, calcite, baroque dolomite, and mega-quartz partially filling the fractures (Figure 7). The fractures occur in intervals with abundant authigenic chert.

Skeletal Grainstone (Figure 5-E): The skeletal grainstone microfacies consists of a diverse fossil assemblage including crinoids, brachiopods, echinoids, bryozoans, ostracods and other disarticulated skeletal fragments. Minor amounts of authigenic dolomite, sparite (sparry calcite cement), idiomorphic quartz, and pyrite (framboidal and cubic) are also present. Extensive chemical compaction has resulted in a pervasive fabric of sutured grain to grain contacts, subtle dissolution seams, and pronounced stylolites. The extensive nature of the chemical compaction may mask the true depositional fabric of more muddy intervals because of micrite solubility, such that packstone intervals could be completely removed at dissolution seams leaving little evidence of their stratigraphic position. Many of the larger crinoid grains (>20 microns) contain intragranular micro-porosity. Other more local porosity includes moldic dissolution pores of various allochems (Figure 5-E) and intercrystalline pores adjacent to idiomorphic quartz. Many of the subtle stylolites also contain segments of dissolution with bitumen in the pore space (Figure 5-F).

STACK

Chert (Figure 6-A): The chert microfacies of the STACK is similar to the NW STACK chert microfacies in the sense of the observed replacement of a previous carbonate by authigenic silica. However, there is a higher volume of spicules in the silica matrix and the replacement is more patchy and as a result many partially replaced crinoids are observed.

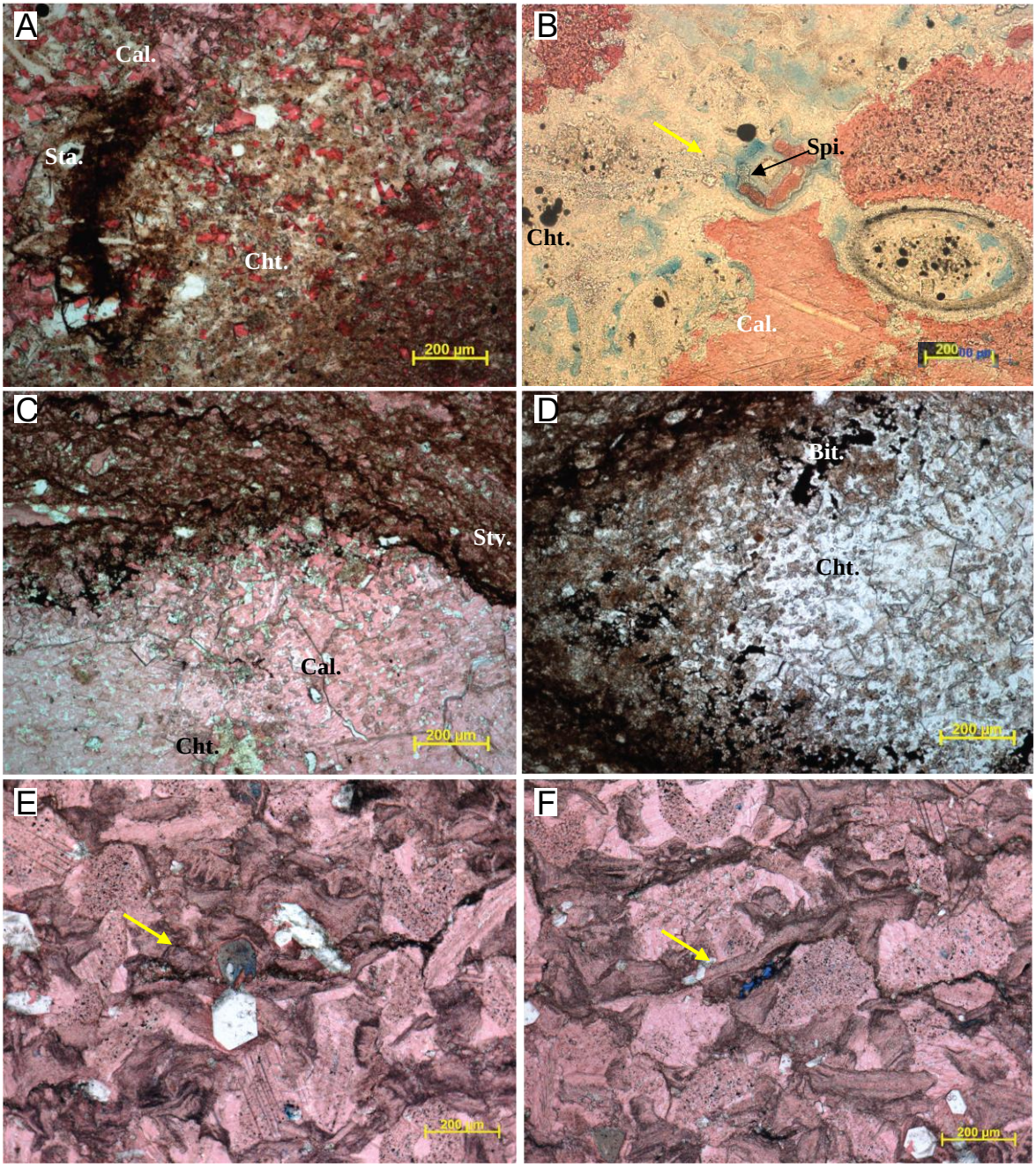

Figure 5: NW STACK Osage microfacies. PPL photomicrographs A-F. Calcite is stained red. Yellow arrows indicate porosity. (A) Chert (Cht.) microfacies showing oil staining and patchy amounts of calcite remaining in various allochems. (B) Chert microfacies showing porosity development in spicules (Spi.) in the silica matrix. (C) Chert nodule bounded by stylolite. (D) Chert nodule with bitumen (Bit.) in the outer portions. (E) Grainstone microfacies with a moldic pore. (F) Grainstone with porosity along a subtle dissolution seam (arrow). Dark material in the seam is bitumen.

Dissolution targets sponge spicules within the silica matrix. The occurrence of the chert microfacies in the STACK is less abundant than the NW STACK and is commonly interbedded with silt-dominated microfacies.

Skeletal Packstone (Figure 6-B): The skeletal packstone microfacies consists of a fossil assemblage of crinoids, bryozoans, brachiopods, ostracods, and other skeletal fragments. The microfacies also contains detrital silt, with authigenic sparite, pyrite and rare dolomite. Some dissolution seams are present, but they are sparse in comparison to the magnitude observed in the NW STACK. Locally, pervasive dissolution of various allochems is observed with significant oil staining at the core scale.

Muddy Wackestone (Figure 6-C): The muddy wackestone microfacies predominantly consists of micrite, detrital silt, sponge spicules, brachiopod spines, disarticulated crinoids, sparite, and pyrite (framboidal and cubic). Little to no porosity is observed in this fine-grained carbonate microfacies. Locally, spicules and brachiopod spines have been replaced by sparite.

Calcitic Siltstone (Figure 6-D): The calcitic siltstone microfacies is poorly sorted and contains moderate to coarse, sub-angular silt, peloids, potassium feldspars, skeletal fragments, pyrite, clay, sparse muscovite, and calcite cement (marine). Little to no porosity was observed during thin section analysis.

Spiculite (Figure 6-E): The spiculite microfacies consists of a configuration of randomly oriented sponge spicules within a matrix of clay. Other grains include detrital silt, potassium feldspar, pyrite and ferroan dolomite (stained blue). Sparse and isolated amounts of moldic pores in spicules are also observed.

Siltstone (Figure 6-F): The siltstone microfacies is defined by a moderately sorted fabric of silt, clay, potassium and plagioclase feldspars, calcite and silica cement, pyrite, and

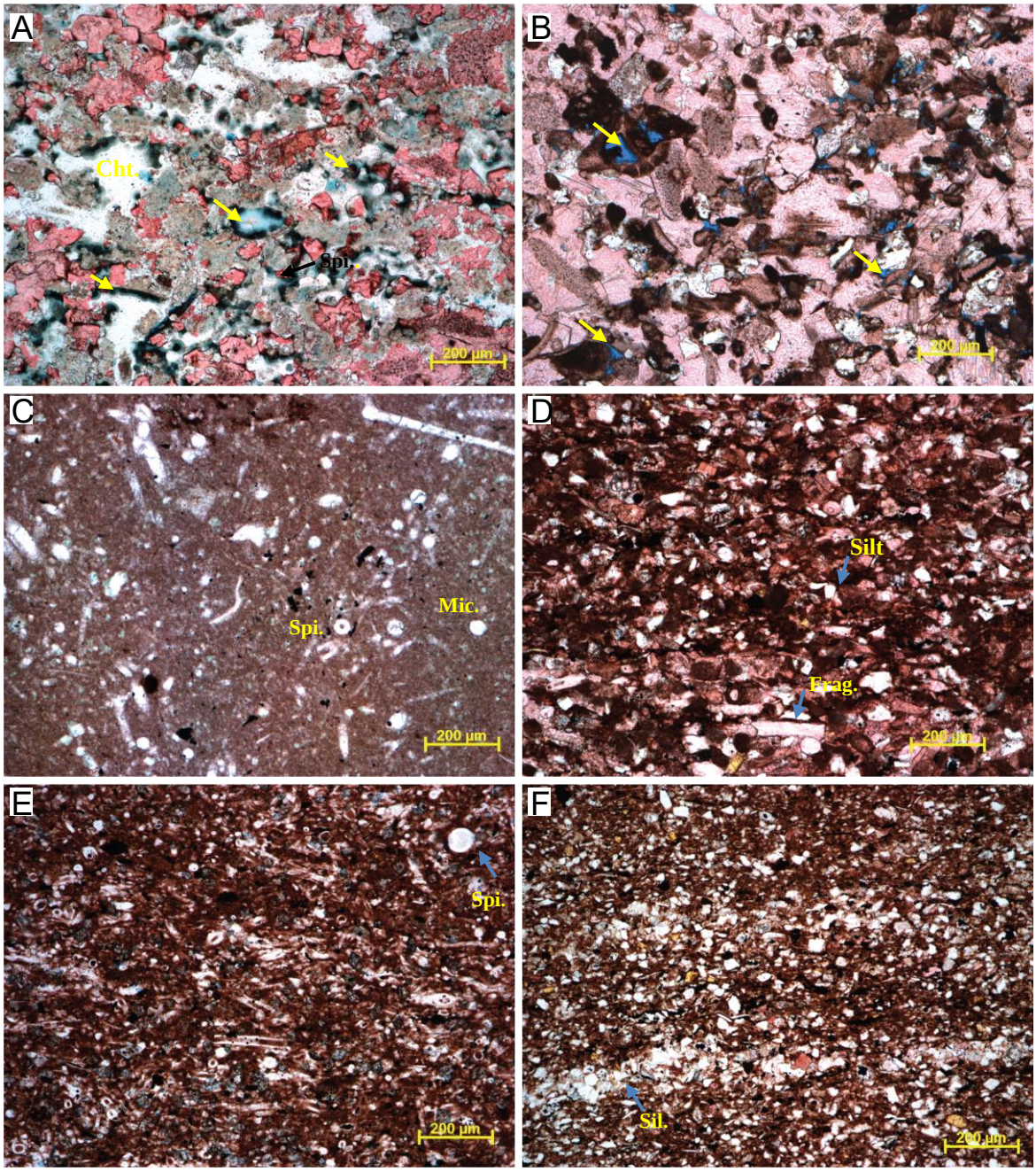

Figure 6: STACK Osage microfacies. PPL photomicrographs A-F. Calcite is stained red. Yellow arrows indicated porosity. Ferroan dolomite is stained blue (E). (A) Chert microfacies with silica matrix and porosity concentrating spicules (Spi.). (B) Packstone microfacies with pervasive dissolution and oil staining of the pores. (C) Muddy wackestone microfacies with an assortment of spicules and other skeletal fragments in a micritc (Mic.) matrix. (D) Calcitic siltstone microfacies with silt and skeletal fragments (frag). (E) Spiculite. (F) Siltstone with minor silica replacement in the matrix.

sparse muscovite. The calcite cement occludes primary pore space and the authigenic silica is locally replacing the matrix. Little to no pores are observed in the siltstone microfacies.

Osage Diagenesis/Paragenesis

Fractures

There are two primary vertical fracture sets that have cross-cutting relationships to constrain the timing of one relative to the other. However, these fracture sets do not contain any cross-cutting interaction with the authigenic phases present in the matrix to constrain the timing of the fractures relative to matrix diagenesis. The earlier fracture set is filled with silica and a later calcite (Figure 7-A). The later fracture set is locally composed of chalcedony on the boundaries and mega-quartz nearing the center (Figure 7-C). The more commonly observed fill is comprised of baroque dolomite on the edges and large syntaxial calcite in the center (Figure 7-A/D). Both fracture sets have evidence for late hydrocarbon migration in the form of solid bitumen present on fracture boundaries and at triple junctions of grain boundaries within the fracture fill.

Matrix

Micritization of various skeletal fragments represents the first diagenetic event in the near-surface environment (Figure 8). The calcite cement that has replaced many crinoids and bryozoan in the matrix of silica is observed with patches of silica replacement suggesting the silicification post-dated the calcite cementation. The phases of dolomite and de-dolomite also within the silica matrix do not have patches of silica replacement indicating the dolomitization events occurred later than silicification. Many silica nodules are bounded by draping stylolites, which constrain the diagenetic events that occur within the silica matrix as early

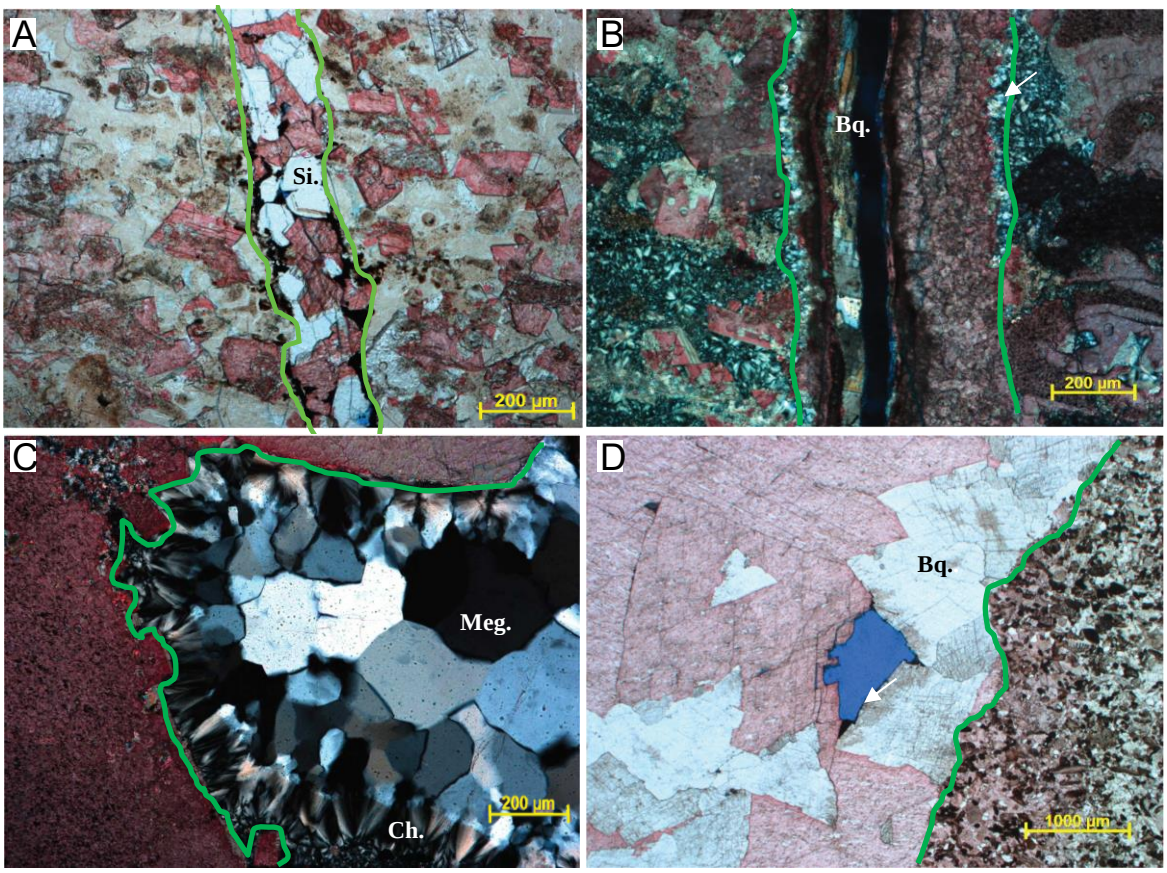

Figure 7: Vertical fractures and fracture fill in the Osage, regionally. PPL photomicrographs A and D. Cross-polorized light (CPL) photomicrographs B and C. Calcite is stained red. (A) Vertical fracture filled with silica and later calcite. The black material within the fracture is bitumen (edge/arrow). (B) Vertical fracture with authigenic phases in the following order: silica (arrow), calcite, and baroque dolomite (Bq.). (C) Authigenic phases filling a void in the following order: chalchedony (Ch.) and mega-quartz (Meg.). (D) Vertical fracture lined with baroque dolomite and a later phase of calcite.

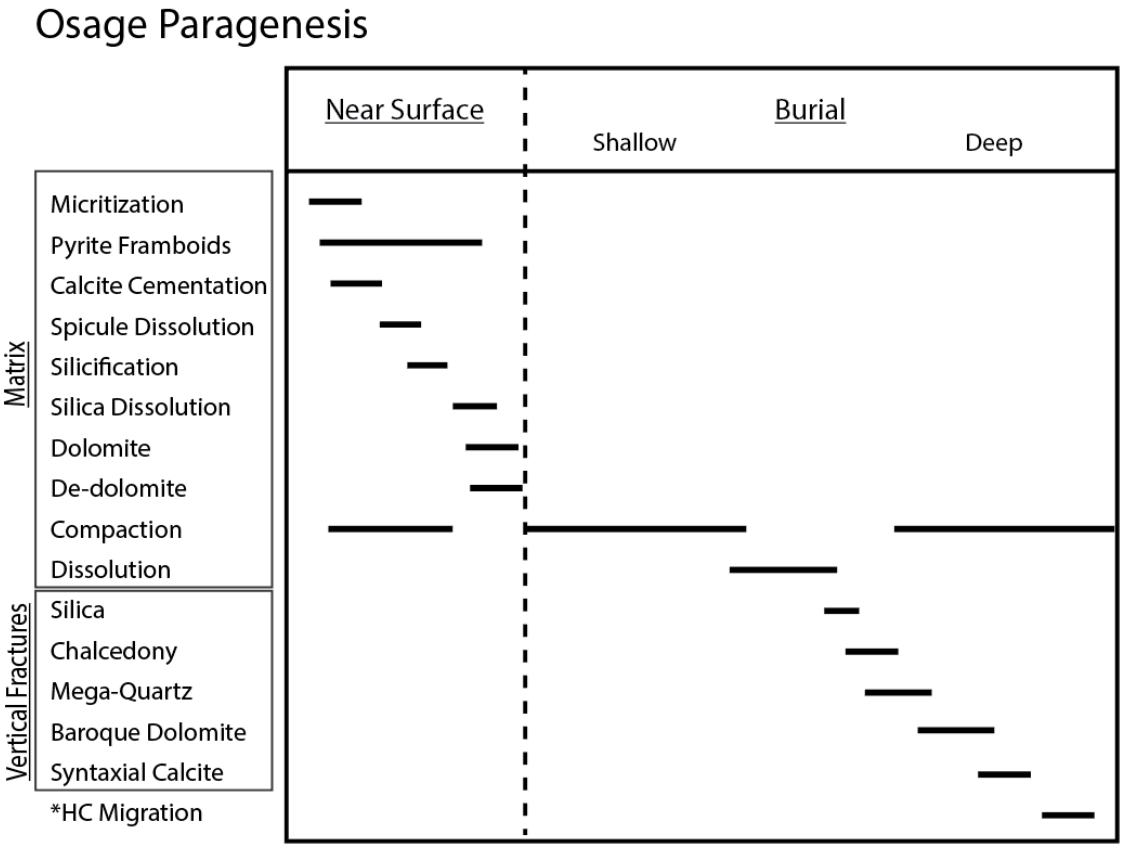

Figure 8: Paragenetic sequence for the Osage showing the relative timing of diagenetic events observed petrographically. The timing of events are constrained by cross-cutting relationships. The boundary between near surface events and shallow burial is defined by the transtion from mechanical to chemical compaction during progressive burial.

near-surface events because they pre- date chemical compaction initiated in the shallow burial regime (Figure 8). There are two dissolution events: the first event dissolved portions of the silica matrix and the second dissolved segments of dissolution seams. There is no direct evidence as to the composition of the soluble material for the second dissolution event, but the fact that the pores match the morphology of the dissolution seams indicates a different genesis that is cotemporaneous with chemical compaction. The relative timing of each diagenetic event is summarized in Figure 8.

Meramec Microfacies

The Meramec in the NW STACK and STACK consists of four primary microfacies, from a reservoir quality perspective (Figure 9). They are: peloidal calcareous siltstone, calcitic siltstone, siltstone, and argillaceous siltstone. Each are defined by volume proportions of framework grains to authigenic phases (Figure 10), pore-types (Figure 11-12) and their relative distribution, and inferred storage and flow capacities.

Peloidal Calcareous Siltstone (Figure 9-A): The peloidal calcareous siltstone consists of sub-angular to sub-rounded, medium to coarse, silt (~35%), calcite (~45%), clay (8%), plagioclase and potassium feldspar (~11%), ferroan dolomite (~3%), and lesser proportions of pyrite and muscovite. These proportions were petrographically estimated and confirmed by XRD analysis. In core, the peloidal calcareous siltstone microfacies is observed in massive, bioturbated, and low angle laminated light gray beds. Calcite is present in peloids, other small skeletal fragments (~<20 microns) and pervasive calcite cement (Figure 10-A). Ferroan dolomite is observed in replacement and cement forms (Figure 10-B). Each of the authigenic dolomite and calcite phases significantly reduce primary porosity. Burrowing commonly reworks the peloidal calcareous siltstone microfacies with clay rich material. Little to no

porosity is observed at the petrographic or SEM scale. This is a result of the pervasive nature of the calcite and dolomite cements; therefore, the intervals with this microfacies are well indurated with little storage or flow capacity.

Calcitic Siltstone (Figure 9-B): The calcitic siltstone microfacies is characterized by sub-angular to sub-rounded, coarse, silt (~43%), calcite (~28%), clay (~13%), plagioclase and potassium feldspar (~12%), ferroan dolomite (~3%), and lesser proportions of pyrite and muscovite. In core this microfacies is variably bioturbated, massive, and locally heterolithically bedded with peloidal calcareous siltstone microfacies (Figure 9-B). The form of the authigenic phases of calcite and dolomite is similar to the peloidal calcareous siltstone microfacies, except the overall volume is less, with more clay in the matrix. The common pore types observed are secondary inragranular pores in dissolved feldspars (Figure 11-A/B, Figure 12-A/B) and secondary intergranular pores between framework grains such as quartz. Each of these pore types range in size from fifteen to fifty microns. Many of the pores are lined with solid bitumen and some are partially occluded by quartz and albite overgrowths (Figure 10-C-F). Stratigraphically, the dissolution within this microfacies is quite variable. Figure 11 E/F highlights portions of the section with enhanced dissolution of an additional cement that is not observed. The intervals with enhanced dissolution are generally accompanied by increased amounts of pores lined with bitumen in thin section and oil staining in core.

Siltstone (Figure 9-C): The siltstone microfacies is defined by sub-angular to sub-rounded, medium to coarse, silt (~46%), clay (~22%), calcite (~15%), plagioclase and potassium feldspar (~14%), ferroan dolomite (~3%), and lesser volumes of pyrite and muscovite. Much of the calcite is in the form of skeletal fragments as opposed to calcite

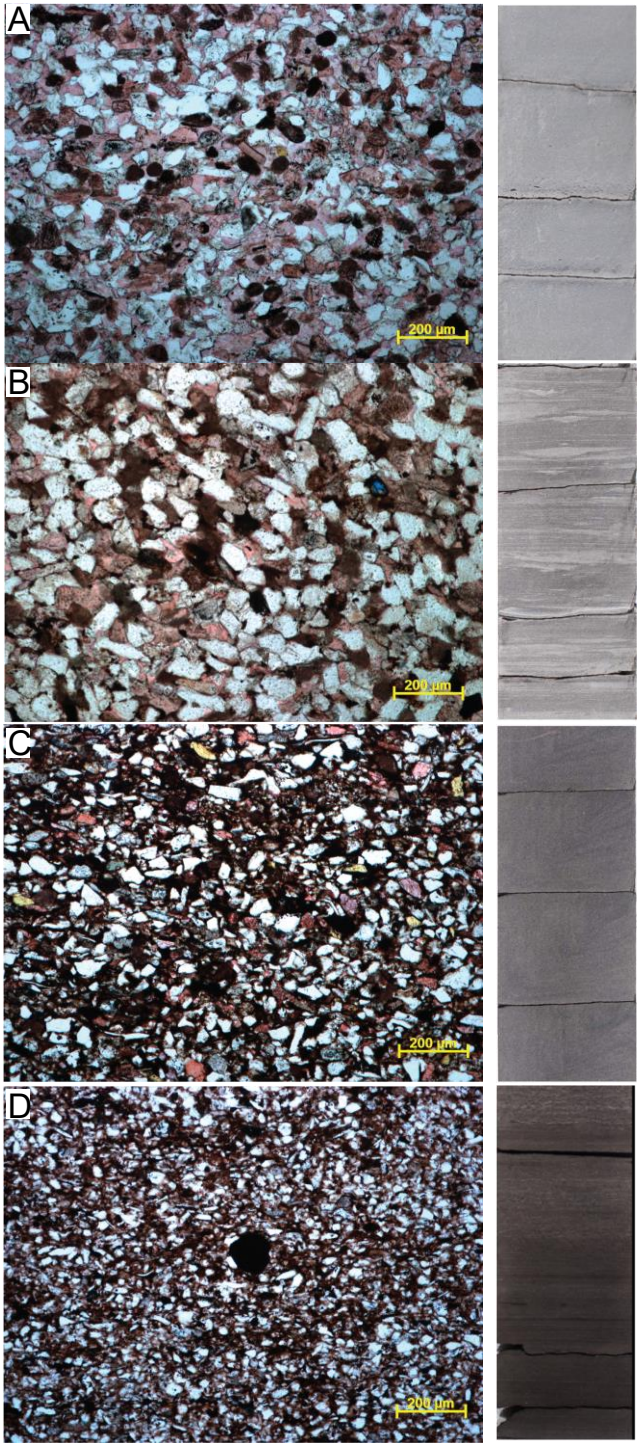

Figure 9: Petrographic (left) and core (right) expression of the primary Meramec microfacies. PPL photomicrographs A-D. Calcite is stained red. (A) Peloidal calcareous siltstone microfacies. (B) Calcitic siltstone microfacies. (C) Siltstone microfacies. (D) Argillaceous siltstone microfacies.

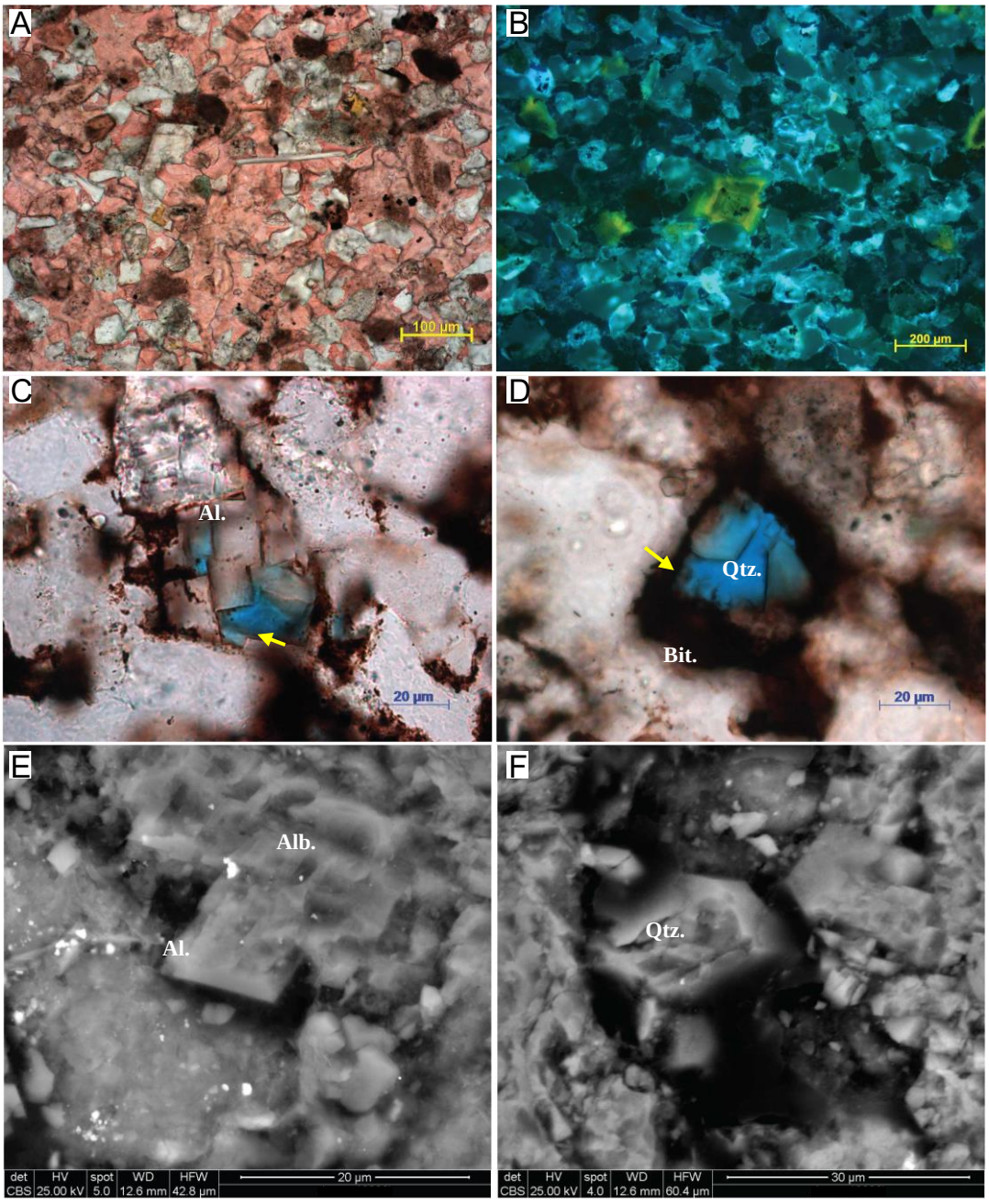

Figure 10: Authigenic phases occluding pore space in the Meramec. PPL photomicrographs A, C, and D. Fluorescent phtomicrograph B with UV light applied. Backscatter SEM images E and F. Yellow arrows indicate porosity. (A) Pervasive calcite cement occluding primary porosity. (B) Ferroan dolomite fluorescing shades of yellow. The zoning of color indicates ferroan zonation within the crystal. (C) Albite (Al.) overgrowth partially occluding pore. (D) Quartz overgrowth (Qtz.) partially occluded pore lined with bitumen (Bit.). (E) Euhedral albite growing off a detrital albite (Alb.). (F) Quartz overgrowth partially occluding pore.

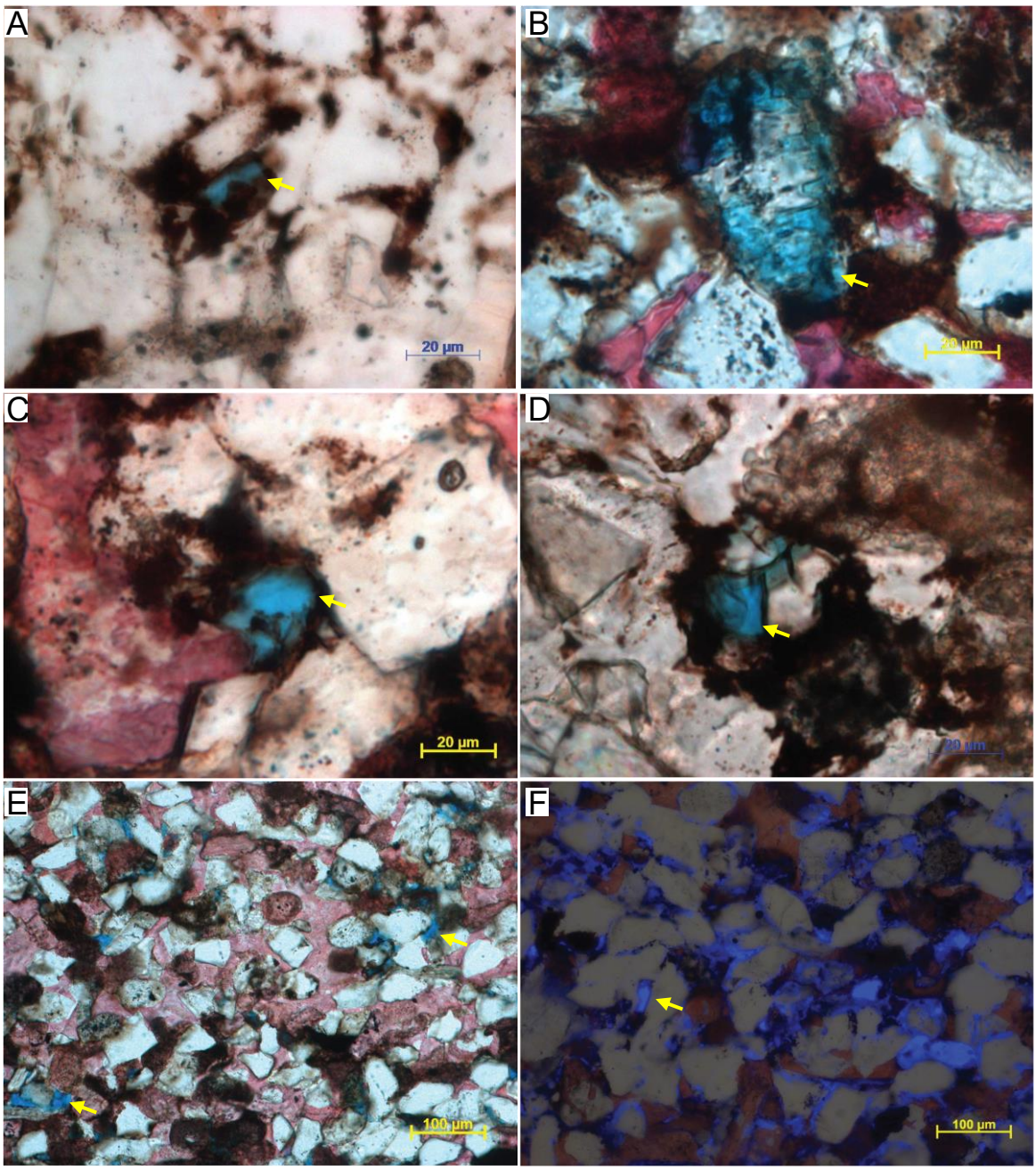

Figure 11: Common pore-types in the Meramec. PPL phtomicrographs A-F. Half UV light and half plain light were applied to photomicrograph F. Porosity indicated by yellow arrows. (A) Intragranular pore in a dissolved feldspar with some bitumen. (B) Dissolved feldspar. (C) Intergranular pore between framework quartz grains. (D) Intergranular pore partially occluded by quartz overgrowths and lined with bitumen. (E) Partial dissolution of the grain in the bottom left. The top right arrow indicates a pore that resides where a cement appears to have once been. Many other pores such as this one occur within this photomicrograph. (F) UV light highlighting microporosity.

cement due to the increase in clay volume decreasing primary porosity for early calcite cementation. There are lesser amounts of dissolved feldspars as compared to the calcitic siltstone facies, but an additional slot-pore is observed in clay, likely illite as illustrated in Figure 12-E. The slot-pore size ranges from 2-20 microns, which is smaller than the range of pore sizes observed in the dissolved feldspars (15-50 microns). In core, the siltstone microfacies is observed in massive, bioturbated, and laminated beds. Bioturbation is most prevalent in the siltstone microfacies as compared to the other microfacies in the Meramec, but the degree of bioturbation is not observed as having a clear correlation to enhanced or decreased porosity.

Argillaceous Siltstone (Figure 9-D): The argillaceous siltstone is characterized by moderate to coarse, silt (~40%), calcite (~10%), clay (~31%), plagioclase and potassium feldspar (~12%), ferroan dolomite (~4%), and smaller amounts of pyrite and muscovite. Small amounts of calcite cement are due to the fact that most primary pore space was likely occluded by clay that the calcite would potentially precipitate in. The argillaceous siltstone is common in laminated beds with rare bioturbation as observed in core. Little to no porosity is observed at the petrographic microscope scale. However, the SEM reveals interstitial nano-porosity within the structure of the clay matrix (Figure 12-C/D). The high abundance of clay-associated interstitial porosity provides enhanced storage capacity, but poor flow properties.

Meramec Diagenesis/Paragenesis

Of the four microfacies defined, the argillaceous, calcitic, and siltstone microfacies contain porosity petrographically observed at the micro and nano-scale. The pore system of the argillaceous siltstone is interpreted to have the greatest pore volume because of the abundance of interstitial porosity held in clay, but it is likely not as effective as the larger

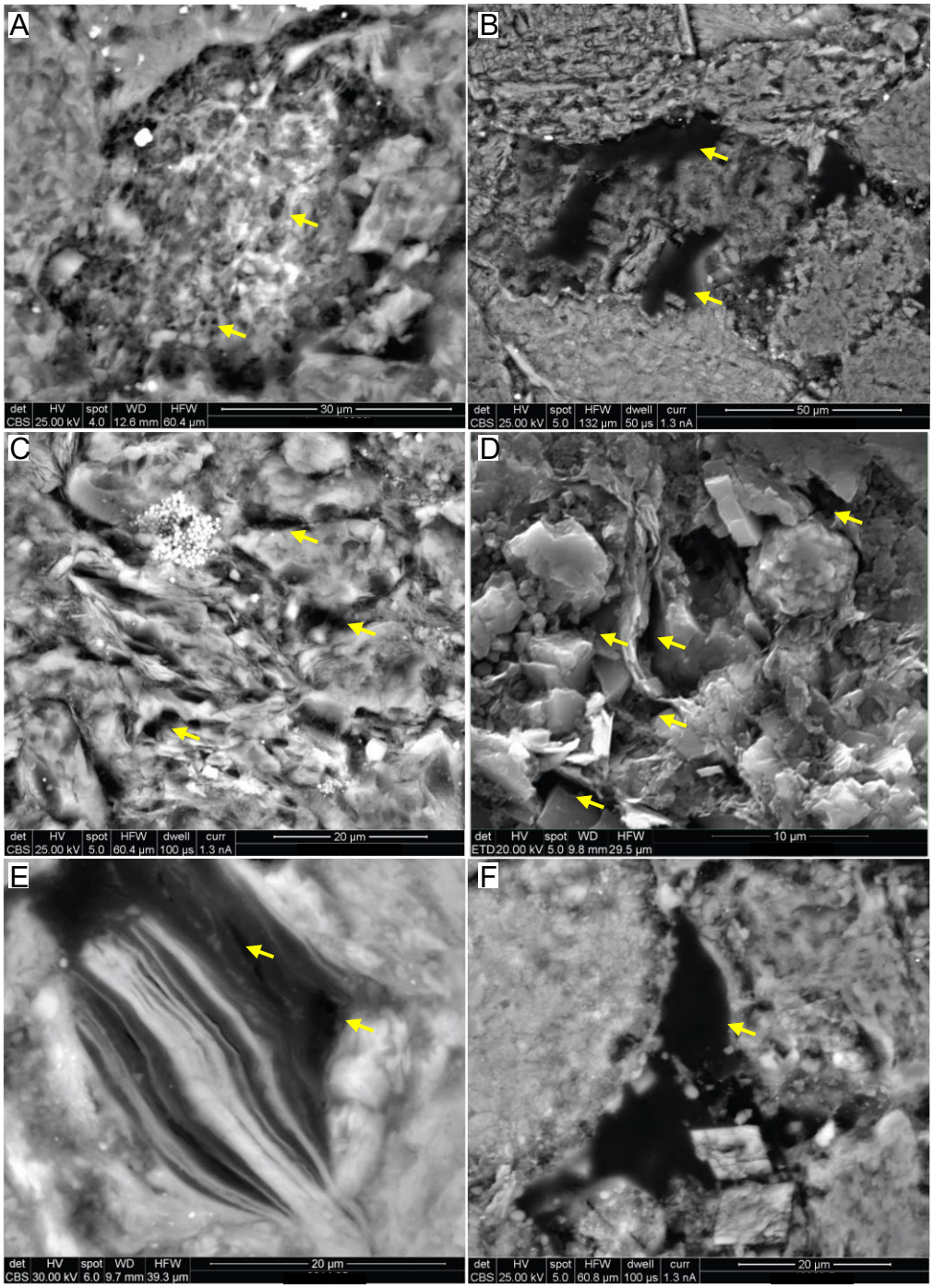

Figure 12: Common pore-types in the Meramec. Backscatter SEM images A-C, E-F. Secondary electron image D. Yellow arrows indicate porosity (A) Partially dissolved feldspar with intragranular pores. (B) More extensively dissolved feldspar with intragranular porosity. (C) Interstital clay porosity. (D) Interstitial clay pores showing the organization of clays influence on pore location. (E) Slot pore within clay and bitumen. (F) Intergranular pore between framework grains also filled with bitumen.

dissolved pores in the calcitic siltstone microfacies. Thus, the argillaceous siltstone should have the best storage capacity and the intervals with greatest dissolution in the calcitic siltstone microfacies should have the best flow properties.

Locally, skeletal fragments display a micritized texture representing the earliest diagenetic event within the near surface environment (Figure 13). “Floating” like silt grains in pervasively calcite cemented microfacies suggest the cementation occurred soon after deposition during the initial stages of mechanical compaction. Framboidal pyrite is interpreted as an early diagenetic event related to sulfate reduction as proposed by Schieber (2011). The secondary pore-types are interpreted to have formed after the near surface diagenetic events, because any coeval pore development would not have been preserved due to the pervasive calcite cementation. Many of the albite and quartz overgrowths cross-cut bitumen lining in various pores suggesting concurrent and continued development during the migration of hydrocarbons.

Mapping

The subsurface correlation of the Meramec, Osage, and Woodford through Woodward, Major, Dewey, Blaine, Kingfisher, and Canadian counties culminated in the stratigraphic interpretation (Figure 14). In the STACK portion of the study area, the Meramec was subdivided into five individual parasequences based on shallowing upward cycles. Each of these parasequences represent regressive facies transitions, except for the observed transgressive cycle in the middle Meramec that is punctuated by an interpreted maximum flooding surface. The overall geometry of the Osage unit resembles a shelf to slope profile (Figure 14) from the NW STACK to STACK. The geometry of the Meramec in the STACK is similar to the proximal topset position of the clinoforms described by Miller (2018) and Price

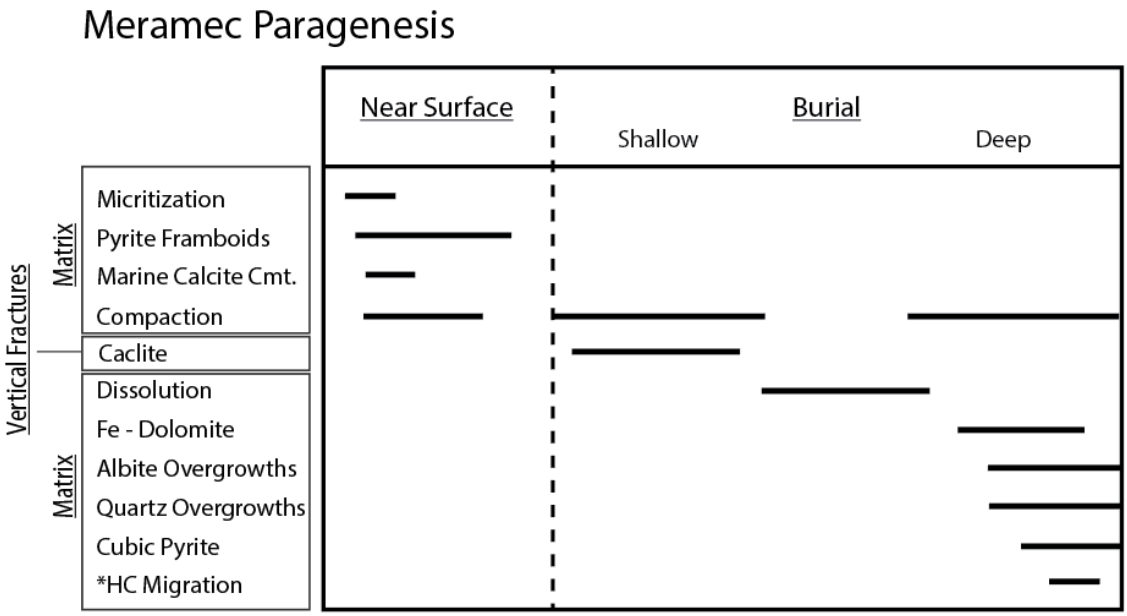

Figure 13: Paragenetic sequence for the Meramec showing the relative timing of diagenetic events observed petrographically. The timing of events are constrained by cross-cutting relationships. The boundary between near surface events and shallow burial is defined by the transtion from mechanical to chemical compaction during progressive burial.

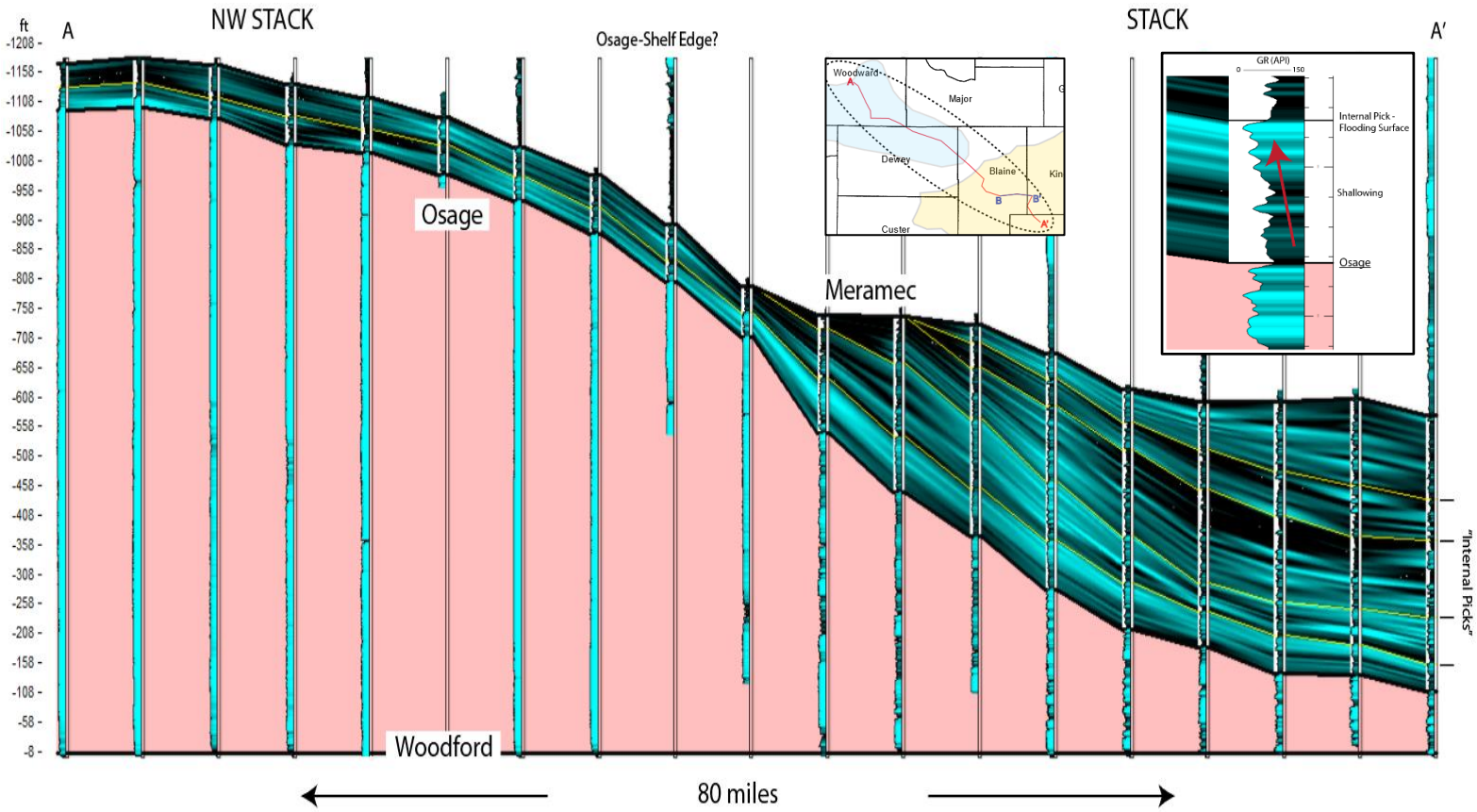

Figure 14: Stratigraphic cross-section from the STACK to the NW STACK highlighting the regional stratigraphic variations. GR is interpolated between each well. Yellow lines indicate internal picks based on interpreted flooding surfaces.

et al. (2017) with an average thickness of five hundred and twenty feet. The transition of the Meramec to the NW STACK exhibits terminations of the upper three parasequences near the shelf edge and as a result the Meramec is locally as thin as fifty feet. The top of the Meramec is regionally expressed as an abrupt increase in resistivity related to the lower conductive clay volume. The termination of individual parasequences in the upper Meramec suggests the top of the Meramec boundary is an unconformable time transgressive surface. At present, this correlation is constrained to log signatures; therefore, an additional chronostratigraphic constraint will add value to the subsurface interpretation.

Hierarchal Clustering Analysis (HRA)

The strategies applied with HRA in the Meramec provided five statistically unique electrofacies (modes) that represent variations in volumetric mineralogy and petrophysical properties. The electrofacies are illustrated stratigraphically in a well from Kingfisher county in Figure 15. Stratigraphic comparison of each microfacies to the equivalent electrofacies found that four of the five electrofacies correlate with the primary microfacies defined for the Meramec (Figure 15). Early petrographic comparisons of the additional electrofacies (illustrated as mode three in Figure 15) yielded little contrasting characteristics with the calcitic siltstone microfacies. However, additional petrophysical analysis (Figure 16) provided insight into the fundamental difference between modes two and three. Mode two displays higher bulk density than mode three, but each possess a similar range of values in neutron porosity. This is interpreted to be a result of locally enhanced dissolution within the calcitic siltstone microfacies. These intervals are characterized by an increased volume of dissolved feldspars as well as more pores lined with solid bitumen. In core, more extensive oil staining is also observed. The difference in bulk density is interpreted to be related to the variations in

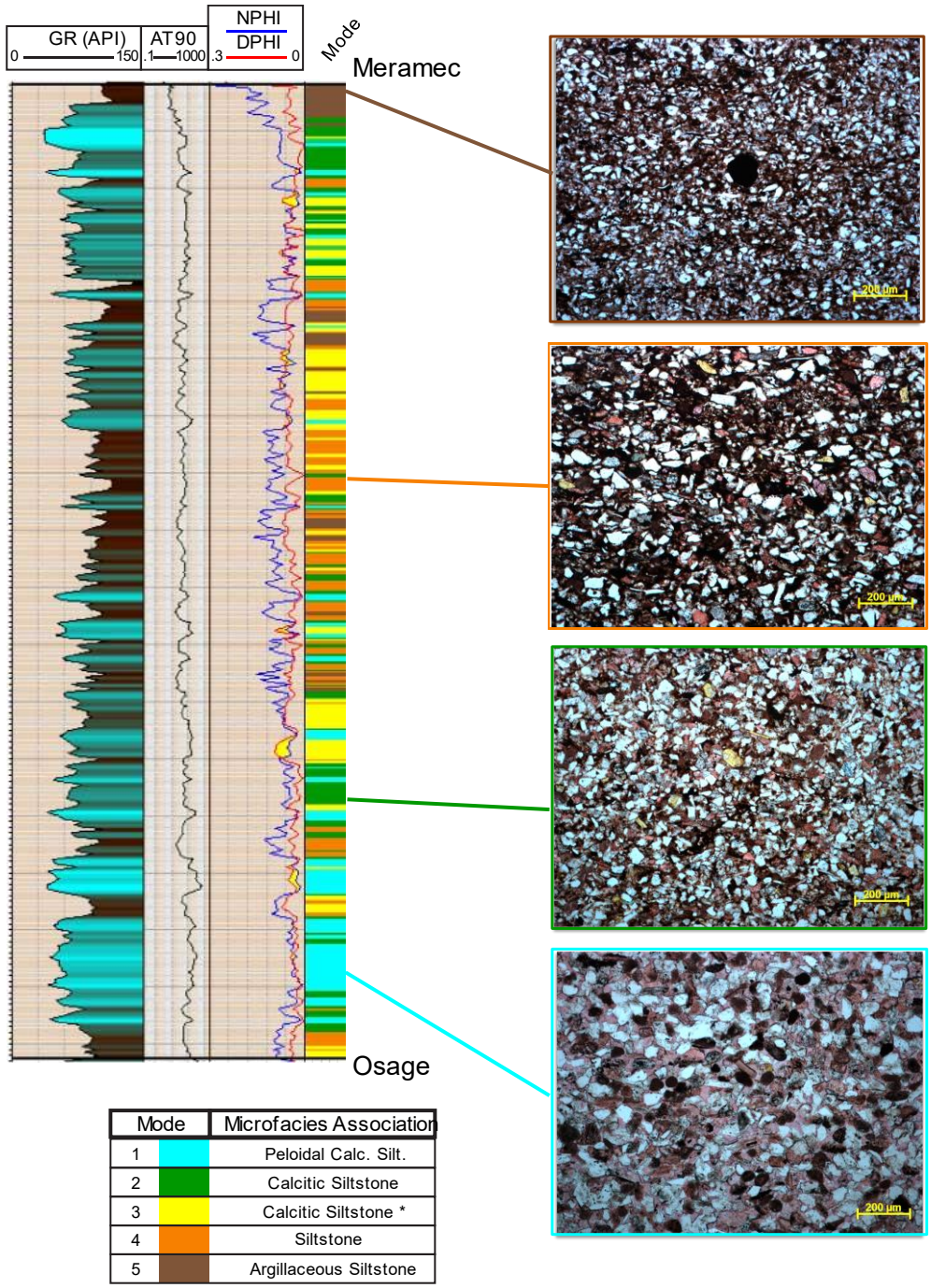

Mode	Microfacies Association
1	Peloidal Calc. Silt.
2	Calcitic Siltstone
3	Calcitic Siltstone *
4	Siltstone
5	Argillaceous Siltstone

Figure 15: Wireline log from Kingfisher county showing the relationship of the electrofacies (left) to the microfacies (right). Left track is GR, the middle-left is AT90, the middle-right is NPHI/DPHI, and the far-right is the electrofacies output. Notice that there is one more electrofacies than microfacies.

pore volume. The similar range in neutron porosity is likely connected to a lower gas density and greater gas in place in the porous intervals masking the true value of the pore volume indicated by neutron porosity. The electrofacies respond to subtle changes in mineralogy and petrophysical properties (Figure 16). Therefore, successful definition of electrofacies provided the ability to predict diagenetic and mineralogic variations through the STACK and NW STACK. Figure 17 highlights the prediction of each of the five electrofacies to thirteen publicly available wells in the STACK and NW STACK. Notice that the STACK contains the greatest volume of the porous calcitic siltstone electrofacies. Each of the lower two parasequences exhibit depositional cycles capped by pervasively cemented peloidal calcareous siltstones. The transition of the lower parasequences to the NW STACK is characterized by less stratigraphic continuity of the electrofacies, representing the proximal shift in the depositional style. The termination of the upper three parasequences near the shelf edge lead to an overall decrease in storage and flow capacities due to the stratigraphic thinning and the loss of effective pore volume held in electrofacies such as the siltstone or porous calcitic siltstone.

Total Porosity and Fluid Saturation Models

The development of the porosity and fluid saturation models helped to confirm the reservoir quality interpretations made within the petrographic portion of the study. Peloidal calcareous siltstone intervals have an average total porosity of two volume percent which results in negligible fluid saturations (Figure 18). These intervals are tight and mechanically indurated as a result of the pervasive calcite cement. The calcitic siltstone intervals contain an average of three percent total pore volume (PHIT) and an additional four percent bulk volume hydrocarbon (BVH). The petrographically similar, but more porous

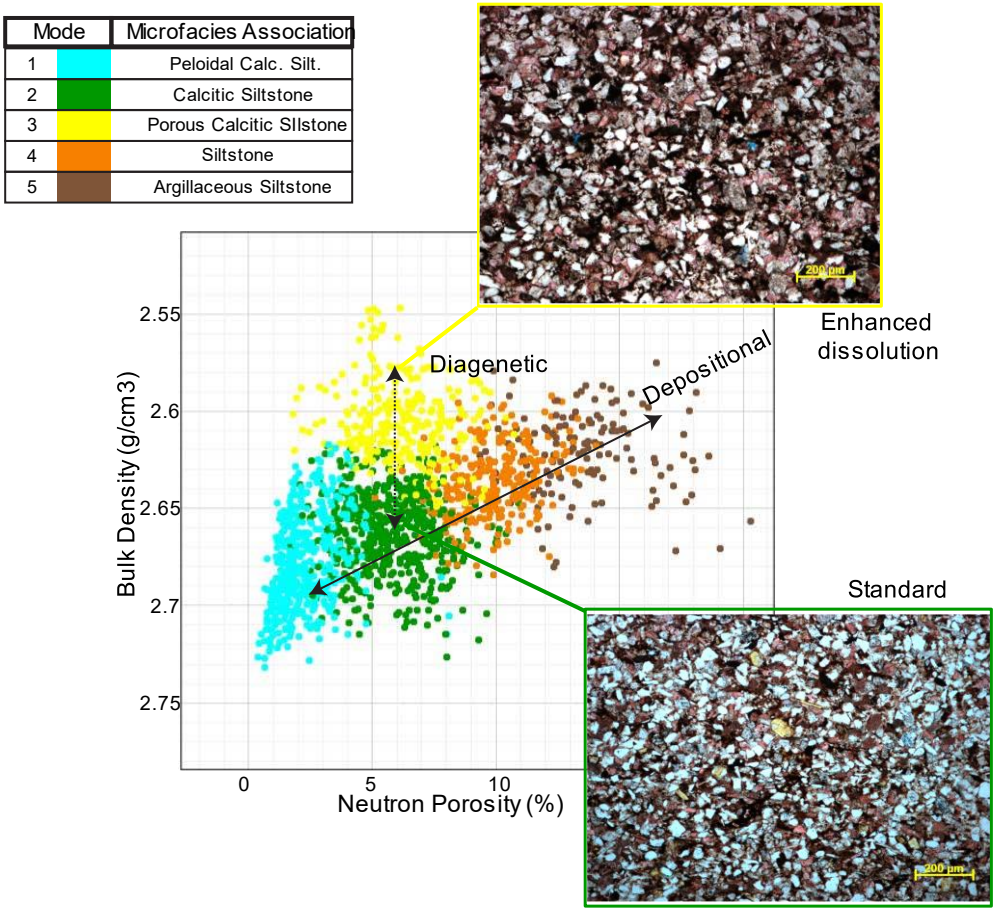

Figure 16: Crossplot of bulk density versus neutron porosity. The trend line that is labeled depostional illustrates the influence of clay versus calcite and the primary microfacies on petrophyscial properties. Notice that each of the four microfacies fall along this trend. The fifth electrofacies falls along an alternative trend that transtions from calcitic siltstone to a calcitic siltstone with enhanced dissolution resulting in the lower bulk density.

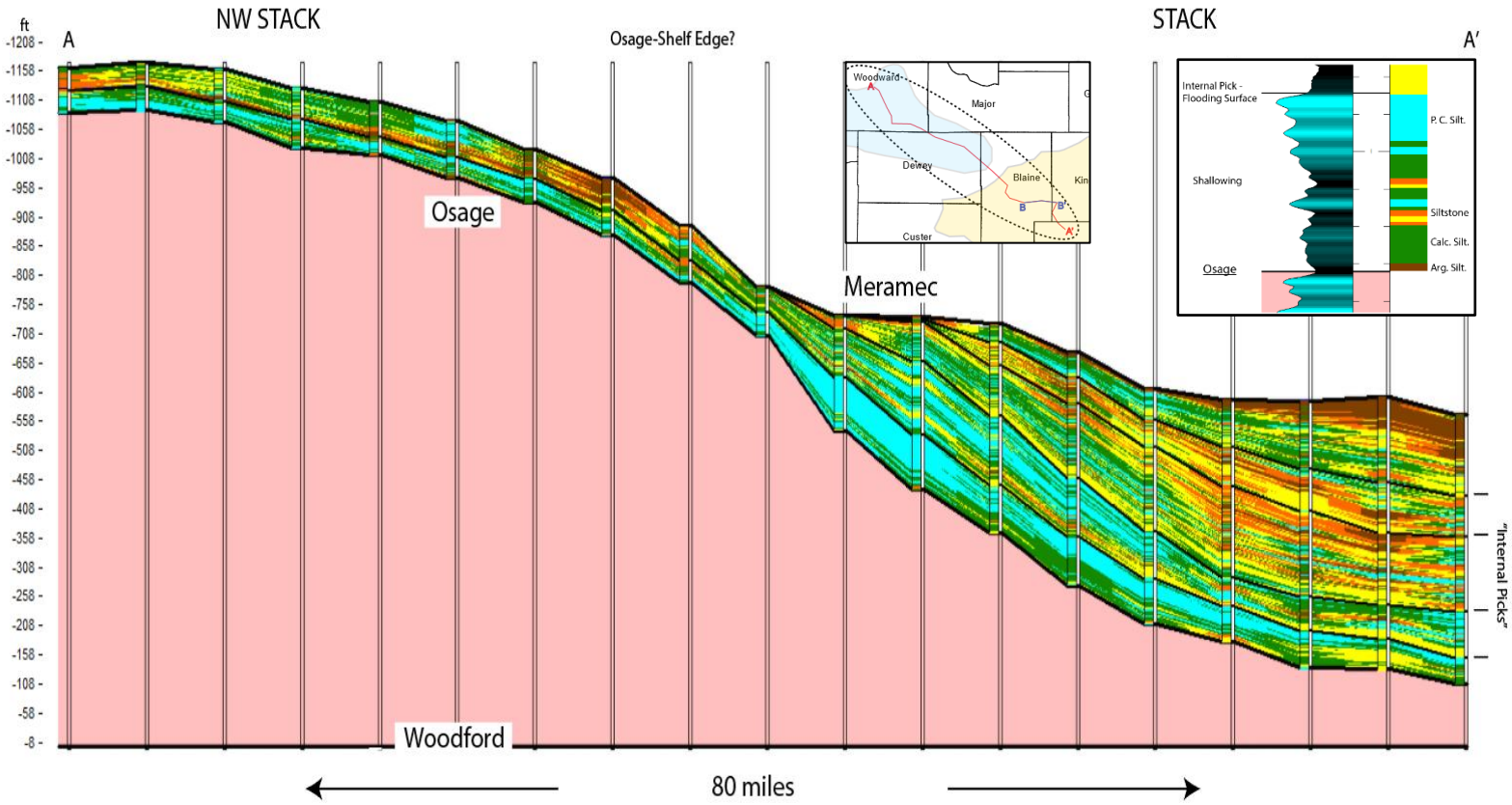

Figure 17: Stratigraphic cross-section from the STACK to the NW STACK highlighting the regional stratigraphic variations. The electrofacies defined in Figure 15 and 16 are predicted to 12 publicly available wells to illustrate the depositional and diagenetic changes regionally.

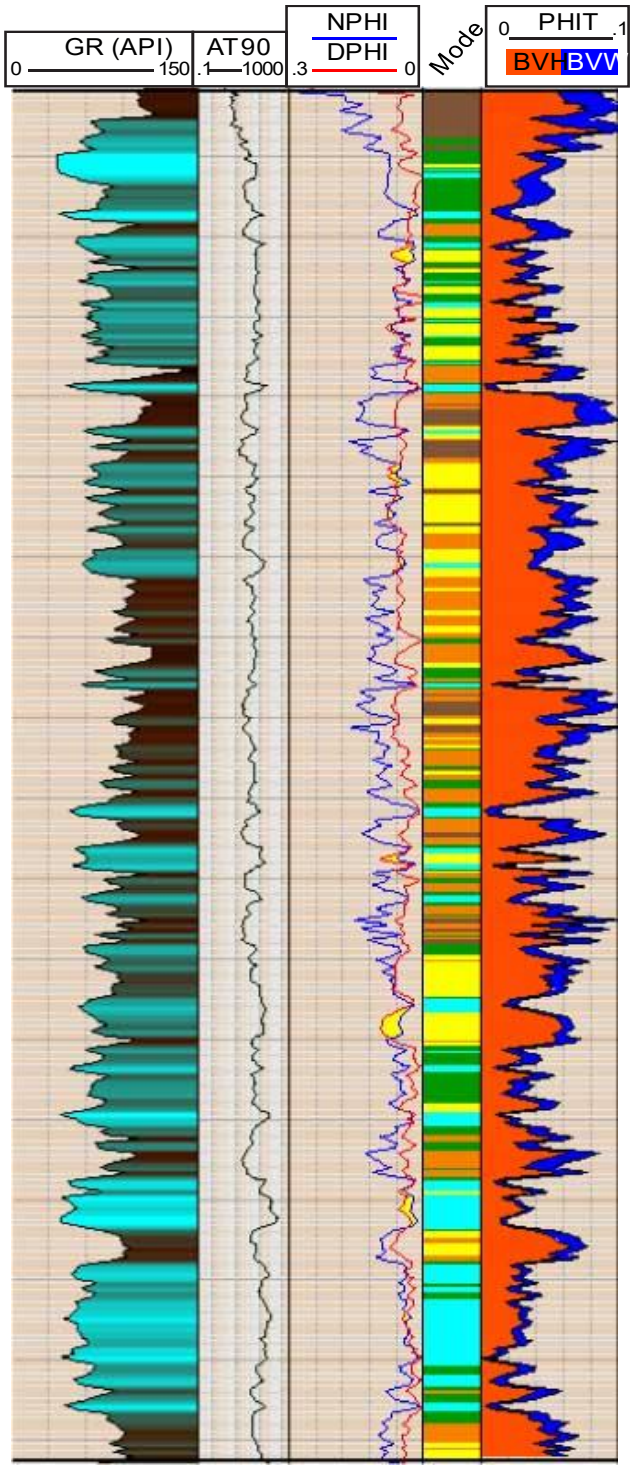

Figure 18: An example of the BVH and PHIT model applied (right track) to a well from Kingfisher county. Notice the electrofacies dependency of the models.

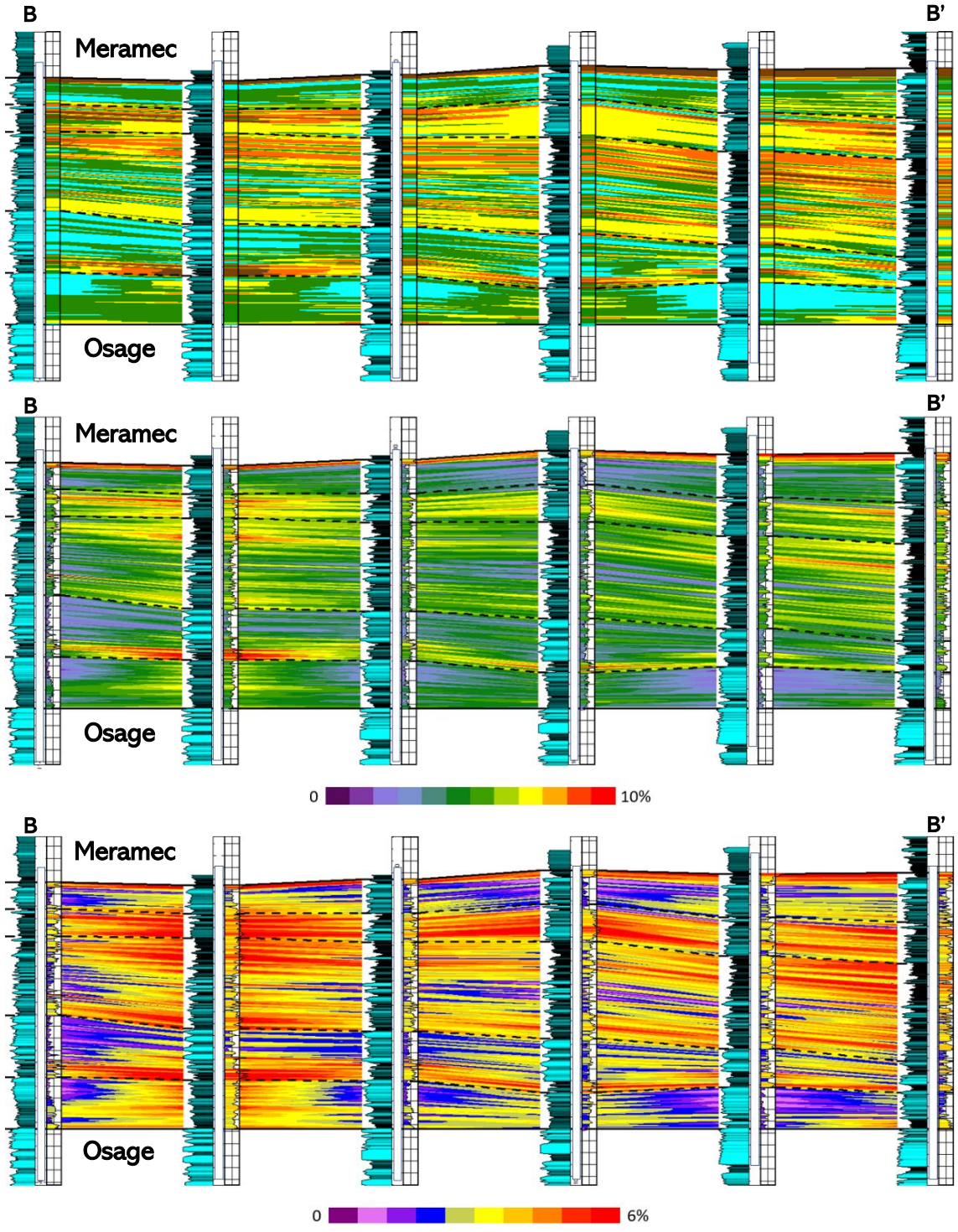

Figure 19: Cross section through portions of Blaine and Kingfisher counties. (Top) Electrofacies predicted and interpolated between wells. (Middle) PHIT is predicted and interpolated between wells. Warm colors indicate high PHIT. (Bottom) BVH is predicted and interpolated between wells. Warm colors indicate high BVH.

calcitic siltstone is characterized by a six percent average PHIT and five percent BVH. Comparatively, the siltstone microfacies also has an average BVH of six percent and a PHIT of five percent. It is interpreted that the subtle variation in porosity between the siltstone and porous calcitic siltstone is due to the additional mode of pores provide by the increased amount of interstitial clay porosity in the siltstone microfacies. However, the BVH between the two is equal; this likely represents the more effective pore network present in the dissolved feldspars of the porous calcitic siltstone. The difference in effective porosity could account for equal fluid saturations with varying PHIT. The argillaceous siltstone represents the microfacies with the highest PHIT of nine percent and a BVH of seven percent. The highest BVH and PHIT present in the argillaceous siltstone suggest quality storage and flow potential, but successfully moving hydrocarbons through interstitial clay nano-porosity remains uncertain. Figure 19 shows a transect through Blaine and Kingfisher counties with the application of the electrofacies, PHIT, and BVH models developed. The internal picks of the Meramec bound the interpolation of the petrophysical properties from well to well. The transitions of electrofacies from Blaine to Kingfisher counties result in enhanced reservoir quality characteristics at B' as compared to B.

Paleomagnetism

Thermal demagnetization of the Meramec and Osage units from a core in Dewey County reveals two magnetic components. A steep component is removed at low temperatures ranging from the NRM (measured at room temperature) to 200°C (Figure 20) and is interpreted as a viscous remanent magnetization (VRM). The steep magnitude of the vertical component (~85°) relative to the modern (~65°) field indicates the VRM may be overlapping with a drilling induced magnetization (Burmester, 1977; Audunsson and Levi, 1989). A

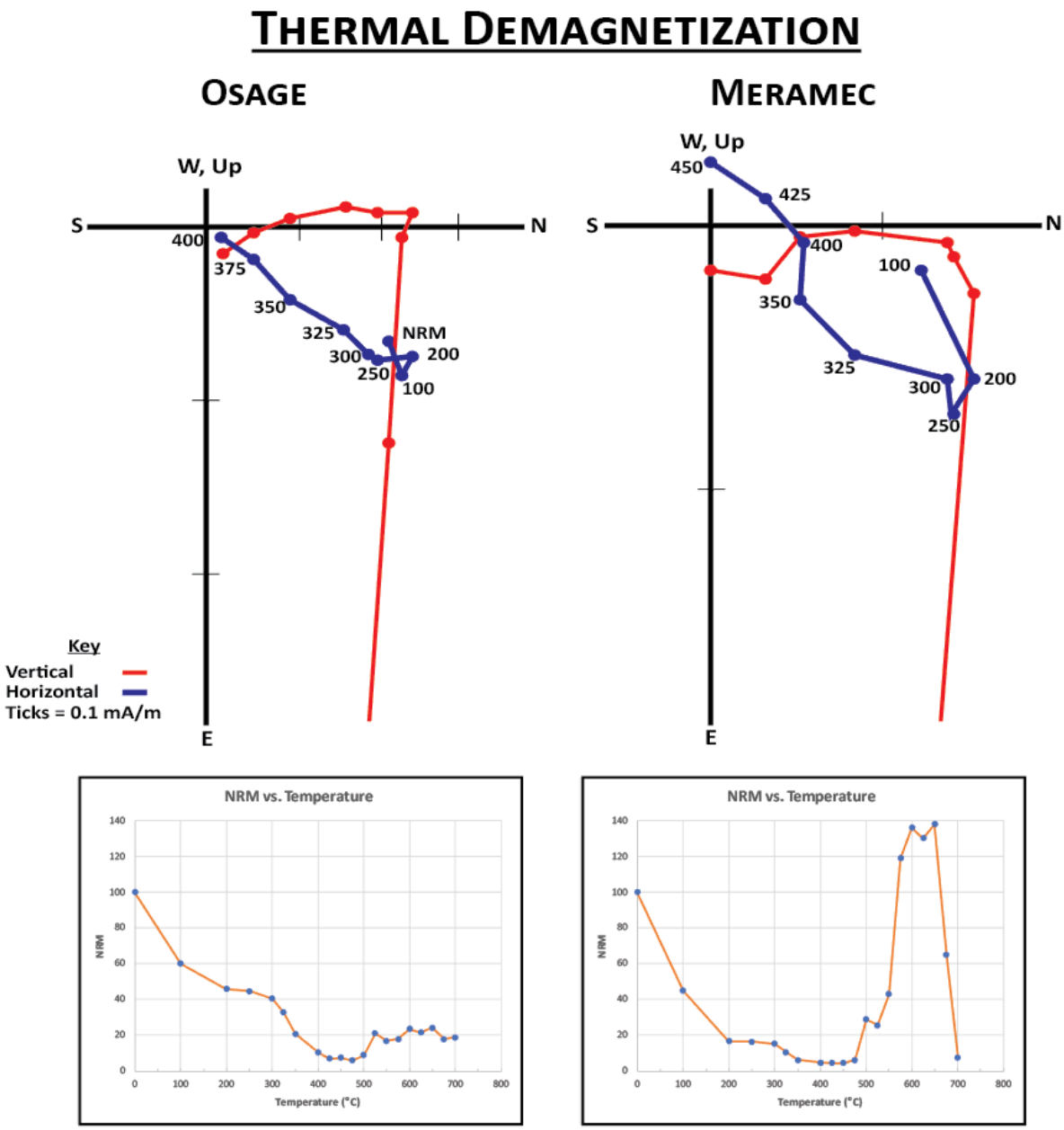

Figure 20: (Top) Representative Zijderveld diagrams for thermal demagnetization in the Meramec and Osage. (Bottom) Representative NRM versus temperature plots from the Meramec and Osage. High temperature steps were removed from the Zijderveld diagrams for illustration purposes.

characteristic remanent magnetization (ChRM) with shallow inclinations is revealed at unblocking temperatures ranging from 250 to 450°C (Figure 20). The average inclination of the ChRM in both units is -12°. At higher temperatures the magnetic intensity increases as a result of pyrite oxidizing to authigenic magnetite (Figure 20) in some specimens. Alternating Field (AF) demagnetization reveals a similar shallow ChRM at an applied field ranging from 30 – 100 millitesla (mT) (Figure 21). However, the average inclination for the ChRM is +14 (Figure 22). It is interpreted that the AF demagnetization did not completely remove the modern component contaminating the ChRM. Therefore, the inclinations from the AF ChRM are not incorporated into the average for the vertical component of the ChRM.

The inclination-only mean (Arason and Levi, 2010) is -12°, with a precision parameter of 28, an alpha 95 (a95) of 6° and an N of 23 samples of both the Meramec and Osage. The mean inclination was compared to the expected inclinations for the study area to date the ChRM (Figure 23). Plotting the a95 values a date ranging from 305 Ma to 295 Ma for the ChRM was identified.

DISCUSSION

Osage Diagenesis

Early paragenesis in the Osage includes pyrite, sparite, silicification, dolomite, and de-dolomite. The chert associated alteration in the Osage indicates that the majority of the early authigenic phases formed during early diagenesis in the near surface with an influence by meteoric processes. The timing of these diagenetic events is constrained by stylolites that often bound the silica matrix. This indicates that the diagenetic events within the silica matrix pre-date chemical compaction and occur in the near-surface

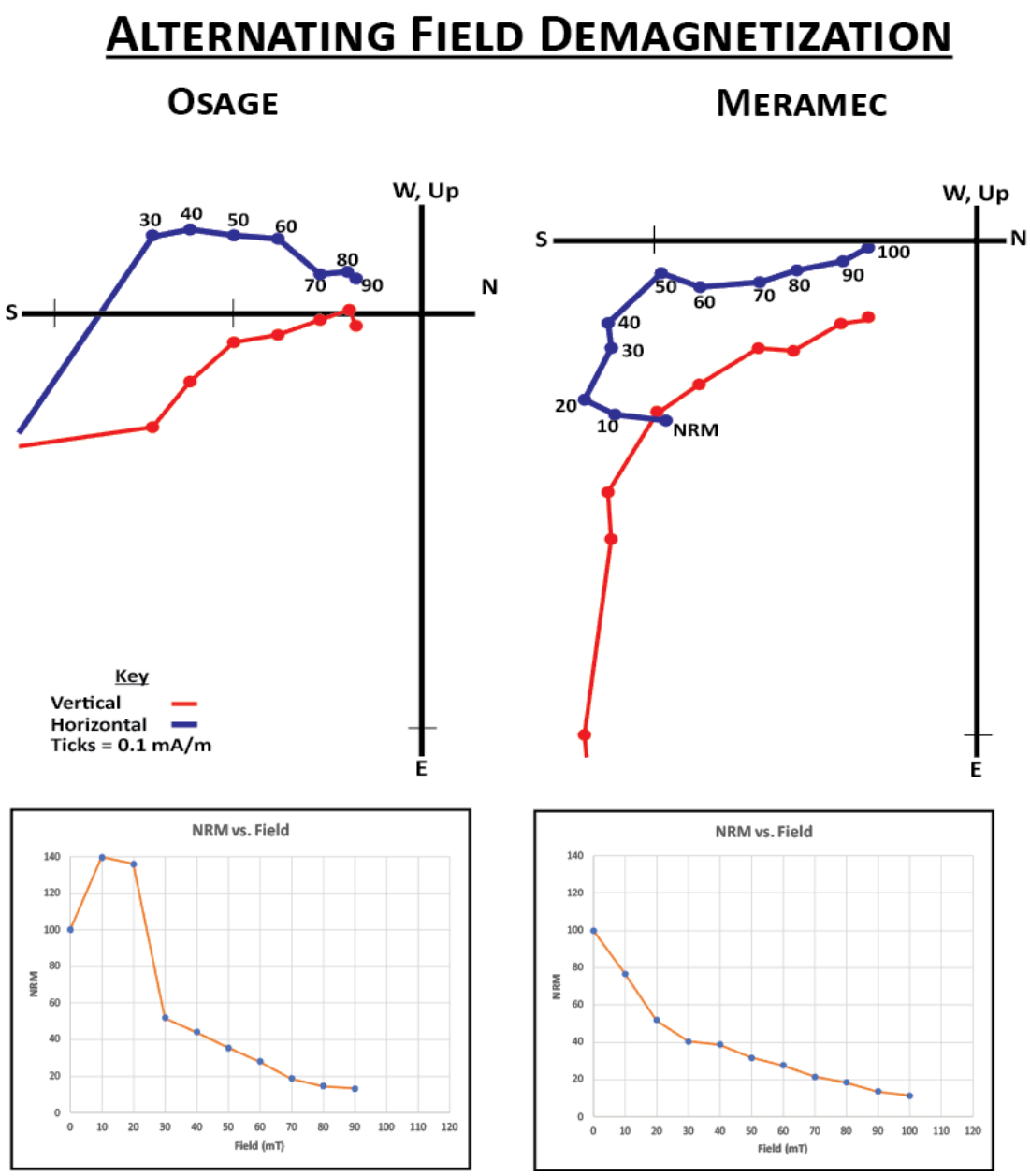

Figure 21: (Top) Representative Zijderveld diagrams for alternating field (AF) demagnetization in the Meramec and Osage. (Bottom) Represenative NRM versus applied field plots from the Meramec and Osage.

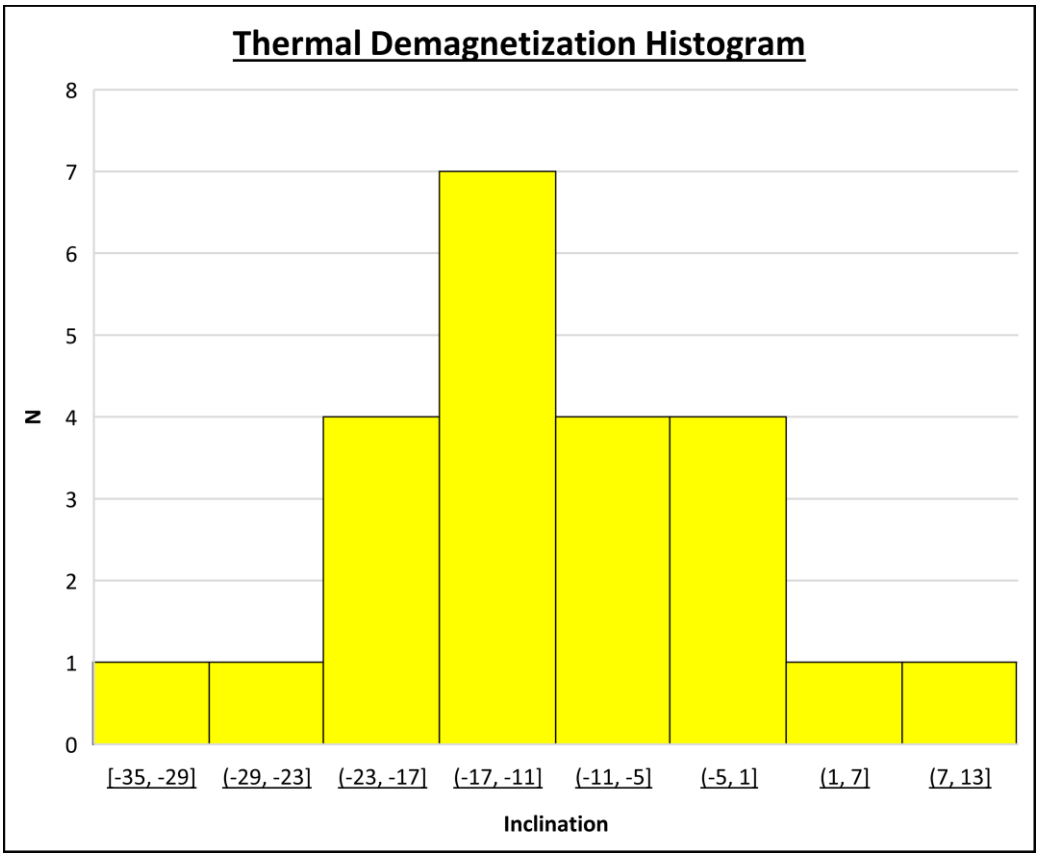

Figure 22: Histogram of the inclination for ChRM from the thermal demagnetization experiments in the Meramec and Osage.

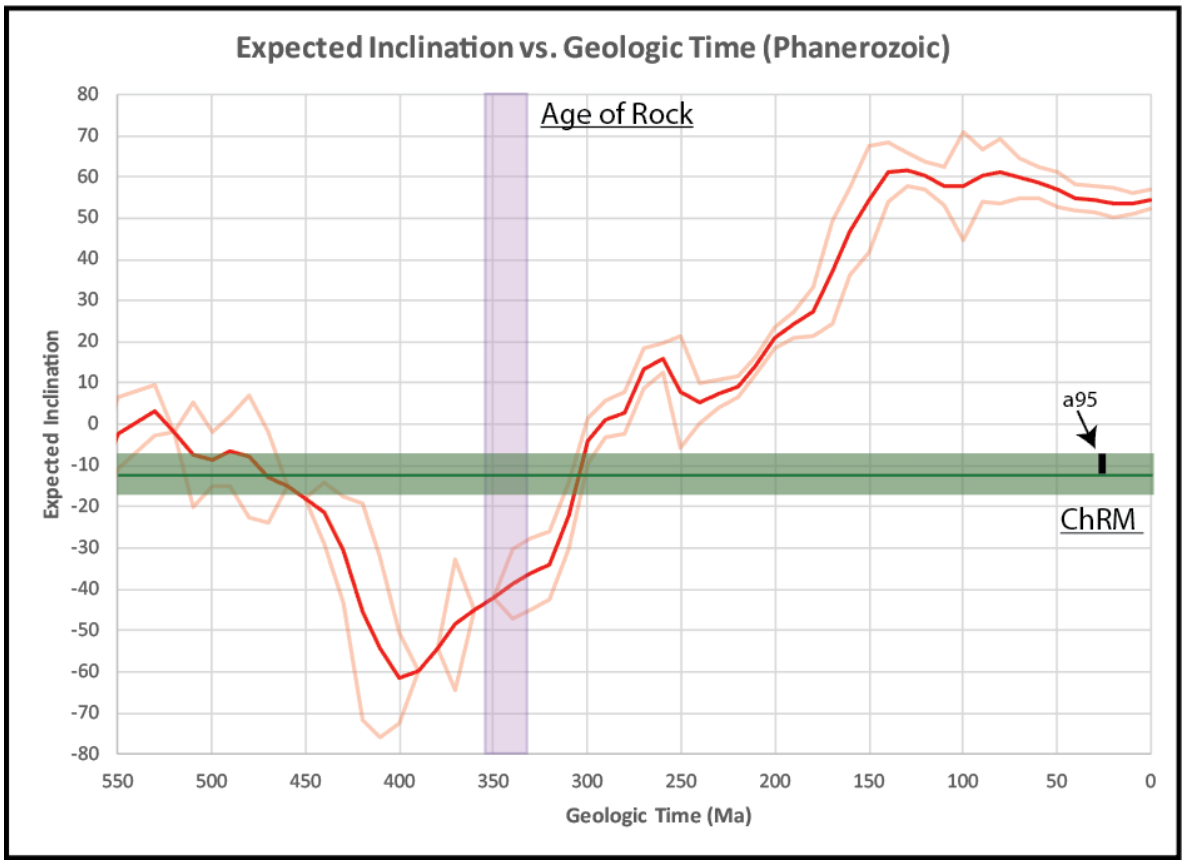

Figure 23: Expected inclination through geologic time plot used to date the characterstic remanent magnetization (ChRM). The dark red is line is the mean inclination and the light red lines are the associated error. The purple box shows the age range for both units and the green box shows the error for the mean inclation (solid green) of the ChRM.

environment. A meteoric origin is also favored by variable amounts of silicification observed that would be difficult to explain without a strong influence by acidic meteoric fluids. Locally, the leaching of sponge spicules serves as evidence to suggest the spicules provided the silica for the variable silicification observed in the STACK and more so in the NW STACK.

The chertification style of diagenesis observed here is consistent with the characteristics of the Mississippian Chat (Rogers, 2001; Watney, 2001) such that significant amounts of calcite were replaced by silica. However, porosity development depends on calcite dissolution in the Mississippian Chat (Rogers, 2001), whereas the chert in this study is preferentially dissolved. This could reflect a fundamentally different groundwater fluid chemistry and depositional setting between the two study localities.

The STACK is in a more distal setting, diluted by clastic detritus, and as a result exhibits a higher volume of silt dominated facies than the NW STACK. Each of the silt dominated facies contain an early marine calcite cement. The alternating styles of marine and meteoric diagenesis along with the mixed carbonate -clastic sequence in the Osage section of the STACK suggest sea level had a major control on the depositional and diagenetic settings.

Mineralized fracture development during burial suggests precipitation of authigenic phases that collectively indicate hydrothermal activity. The phases include authigenic mega-quartz, baroque dolomite, and later calcite in fracture fill. These coincide with hydrothermal phases outlined by Goldstein and King (2014) as representing localized hydrothermal fluid flow that may be related to Laramide structural development. These fracture fill phases are not present within the matrix; therefore, sub-vertical fractures probably provided the principal conduit for fluid flow and stratiform hydrothermal fluid flow was unlikely. The variation in

orientation of these fracture sets could be related to subtle rotations of the stress field during progressive burial.

Much of the porosity in the Osage is secondary in origin, in spicule-rich intervals, and depends on the influence of meteoric groundwater during early diagenesis. This results in moldic porosity in spicules and intercrystalline porosity within the microcrystalline silica matrix. Local grainstone intervals also suggest an episode of much later dissolution where porosity is developed along stylolites and as molds within various skeletal fragments. The dissolution along the stylolites indicates the material accumulated along the seam and was later dissolved. The only evidence for the source of later dissolving fluids is in an interval where a sub-vertical fracture cross-cuts the porous grainstone section. This fracture contains hydrothermal baroque dolomite and calcite suggesting the hydrothermal fluids may have been corrosive enough to result in locally enhanced porosity. Although this later event resulted in anomalous pore volumes (visually estimated <10%) the distribution is significantly less consistent than the meteoric fluid originated porosity in chert.

Meramec Diagenesis

The Meramec represents a different depositional setting as compared to the Osage with a more direct input of clastic detritus near fair-weather to below storm wave base (Price et al., 2017; Miller, 2018). As a result, the near surface style of diagenesis transitions from the meteoric to marine realm with fewer early authigenic phases present. The primary early authigenic phase variably occurring across each microfacies is a marine calcite cement. The early and pervasive nature of the cement as observed in this study and documented in other marine settings is significantly detrimental to primary porosity and permeability (Fontana et al., 1986; James, 1992; Mansurbeg et al., 2009). The presence of floating like silt grains

within the cement suggest an early and syn-sedimentary origin (Ulmer-Scholle et al., 2015). The calcite cement is likely the low-magnesium end-member of calcite as high-magnesium calcite is relatively unstable past surface conditions (Molenaar, 1990). Although there is no direct textural evidence for the inversion or replacement of aragonite with low-magnesium calcite, the high-magnesium seawater present during the time of deposition (Stanley et al., 2002) suggests the replacement most likely occurred.

The shallowing upward parasequences (Figure 17) also exhibit an increased volume of skeletal fragments as the microfacies transition from clay dominated argillaceous siltstones to peloidal calcareous siltstones. The shallow peloidal calcareous siltstone is characterized by the most pervasive calcite cement of the primary microfacies in the Meramec. This is a result of high initial primary porosity and an abundance of intra-basinal skeletal fragments. The skeletal fragments can (1) provide a nucleation surface for calcite cementation (Carvalho et al., 1995; Morad, 2010) and (2) can act as a direct source for calcite cementation if dissolved during the diagenetic evolution of the sediment (Al-Ramadan et al., 2005; Morad, 2010). Calcite cementation is common below flooding surfaces (or upper portion of a shallowing parasequence as the section can be comprised of lag deposits rich in bioclasts (Ketzer et al., 2002; Ketzer and Morad, 2006; Morad, 2010). These deposits in the Meramec may represent reworking of the carbonate substratum by storms (Miller, 2018).

Burial diagenesis in the Meramec is characterized by variable dissolution of feldspars in the primary microfacies. The dissolution event is identified as burial in origin as any dissolution in the near-surface environment would likely be occluded by calcite cement. Potential mechanisms for the source of the dissolving fluids could be illitization (Ulmer-Scholle et al., 2015) or early oil maturation (Welch and Ullman., 1996; Ehrenberg et al.,

2001). Quartz and albite overgrowths are observed partially occluding pores in between framework grains. Many of the overgrowths are hosted on a detrital framework grain with syntaxial monocrystalline overgrowths. Quartz overgrowths are more common and generally form above 60-80 °C (Ulmer-Scholle et al., 2015, Bjorlykke and Jakobsen, 1993; Walderhaug, 2000), whereas albite overgrowths are more locally observed and reported in the North Sea to have formed coeval with quartz overgrowths around 110 °C (Nedkvitne et al., 1993). The source of the elements in the overgrowths could be derived from the products of feldspar dissolution (Ulmer-Scholle et al., 2015). Some overgrowths display growth in the pore cross-cutting the bitumen lining and others display bitumen lining the growth, thus, suggesting each are relatively coincident with hydrocarbon migration.

Apart from interstitial clay porosity primarily observed in the argillaceous siltstone microfacies, much of the remaining porosity is secondary in origin and related to the later burial dissolution event. The magnitude of dissolution is greatest in feldspars of the calcitic siltstone microfacies. It is interpreted that this is a result of adequate clay volume that partially protected primary porosity from cementation. However, the volume of clay is low enough to still have a sufficient quartz silt to clay ratio to promote a framework with less tortuosity, for later fluid flow, as opposed to the clay dominated argillaceous siltstone. Therefore, there is a clear correlation between the magnitude of secondary porosity development and the volume of clay to calcite as controlled by the depositional facies.

The style of diagenesis observed in the Meramec suggests the fundamentals of sandstone diagenesis as proposed by Hayes (1979) do not wholly apply to a mixed carbonate-siliciclastic depositional setting. As opposed to the loss of primary porosity and permeability by compaction, the Meramec loses primary porosity and permeability by marine calcite

cementation. This style of primary porosity loss highlights the significance of calcite solubility as providing a readily available source for pervasive calcite cementation. Additionally, it seems as if the principal control of diagenetic reactions within the Meramec is not simply the given path of sediments from source to sink, but rather a first-order control by sea-level fluctuations influencing the volume of terrigenous input by silt and clay. The most applicable fundamental process of sandstone diagenesis aligned with the characteristics of the Meramec is the development of secondary porosity at depth.

Reservoir Quality

The correlation of microfacies stratigraphic occurrence to electrofacies represented a unique strategy of connecting scales of observation petrographically and petrophysically. Each facilitated insightful observations of the mineralogy, porosity, and hydrocarbon potential. The following is a ranking of electrofacies from low to high reservoir quality through the interpretation of results from the petrography and HCA, as well as the porosity and fluid saturation models.

Peloidal Calcareous Siltstone: The peloidal calcareous siltstone displays very low volumes of porosity due to pervasive calcite cementation. The pervasive nature of the cement suggests high primary porosity and added nucleation sites by skeletal fragments may have had an influence. At the reservoir scale, these intervals may have stagnated vertical flow during hydrocarbon migration and may presently suppress fracture propagation heights during hydraulic fracturing.

Calcitic Siltstone: The calcitic siltstone represents the standard magnitude of dissolution porosity in feldspars and intergranular porosity between framework grains. The standard amount of dissolution results in low storage capacity; therefore, small amounts of

hydrocarbons are present in this microfacies.

Argillaceous Siltstone: The argillaceous siltstone has an abundance of storage capacity held in interstitial clay porosity. However, the observed nano and micro-scale size of the clay associated porosity is concerning for the overall movability of hydrocarbons.

Porous Calcitic Siltstone: The porous calcitic siltstone displays the largest amount of dissolved feldspars and contains pervasive oil staining. This electrofacies is inferred to have the best flow capacity as a result of the larger pore sizes provided by enhanced dissolution.

Siltstone: The siltstone is characterized by a mix of clay associated porosity and dissolution pores in feldspars. The mix provides a bi-modal pore system that will benefit the storage capacity and movability of hydrocarbons. Therefore, it is interpreted that the siltstone will have the greatest drained volume of hydrocarbons during production in the Meramec, both as a flow unit and a carrier bed.

The primary microfacies and diagenetically enhanced intervals of the Meramec are recorded in the response of wireline logs. HCA application revealed the grouping of such responses into electrofacies providing a robust petrophysical characterization of rock to log interactions. The electrofacies were predicted to publicly available wells to highlight the potential for predicting reservoir quality. The electrofacies prediction could also provide the basis for other studies incorporating three-dimensional reservoir models and simulations.

Paleomagnetism

The maximum unblocking temperatures of the ChRM indicate the magnetization resides in magnetite. The AF demagnetization of the ChRM are consistent with this interpretation. The statistical overlap of inclinations between the Meramec (12.6°) and Osage (10.6°) suggest the ChRM is not unit or facies specific. However, the ChRM is not commonly

observed in the Meramec because it is obscured by the creation of new magnetite from pyrite during thermal demagnetization. Within the study area, the temperature reached by the Meramec and Osage associated deposits during the acquisition of the ChRM was around 90 °C (Figure 24). A thermo- viscus remanent magnetization would require maximum unblocking temperatures of around 330 °C for single domain magnetite (Pullajah et al., 1975) and 350 – 400°C for multidomain magnetite (e.g., Kent, 1986). Both are lower than the unblocking temperatures of the ChRM. Therefore, the ChRM is interpreted as a chemical remanent magnetization (CRM).

The CRM was acquired during a time of rapid subsidence (~300 Ma) related to Ouachita orogeny (Figure 24). Hydrothermal fluids related to the Ouachita orogeny have been reported from the Woodford Shale in the Anadarko Basin and interpreted to have caused the acquisition of a CRM in the Ardmore Basin (Roberts, 2017). In this study, hydrothermal alteration is specific to the Osage, so orogenic activity is not a likely origin for the CRM in both units. Therefore, a burial mechanism is more likely to have caused the CRM. Burial mechanisms such as illitization, (Hirt et al., 1993; Katz et al., 1998; Kennedy et al., 2002; Woods et al, 2002) and hydrocarbon emplacement (Elmore and Crawford, 1990; Elmore et al., 1993) have been cited as forming CRMs held in magnetite. Smectite and illite are variably present in the Meramec, but clay is rare in the Osage. Thus, the most appropriate mechanism to support the origin of the CRM is hydrocarbon emplacement as both the Osage and Meramec have solid bitumen in pore space indicating the migration of hydrocarbons through each unit.

Based on the thermal evolution of the Meramec and Osage (Figure 24), the earliest oil generation was probably around 310 Ma (60 °C). The CRM is approximately 300 Ma;

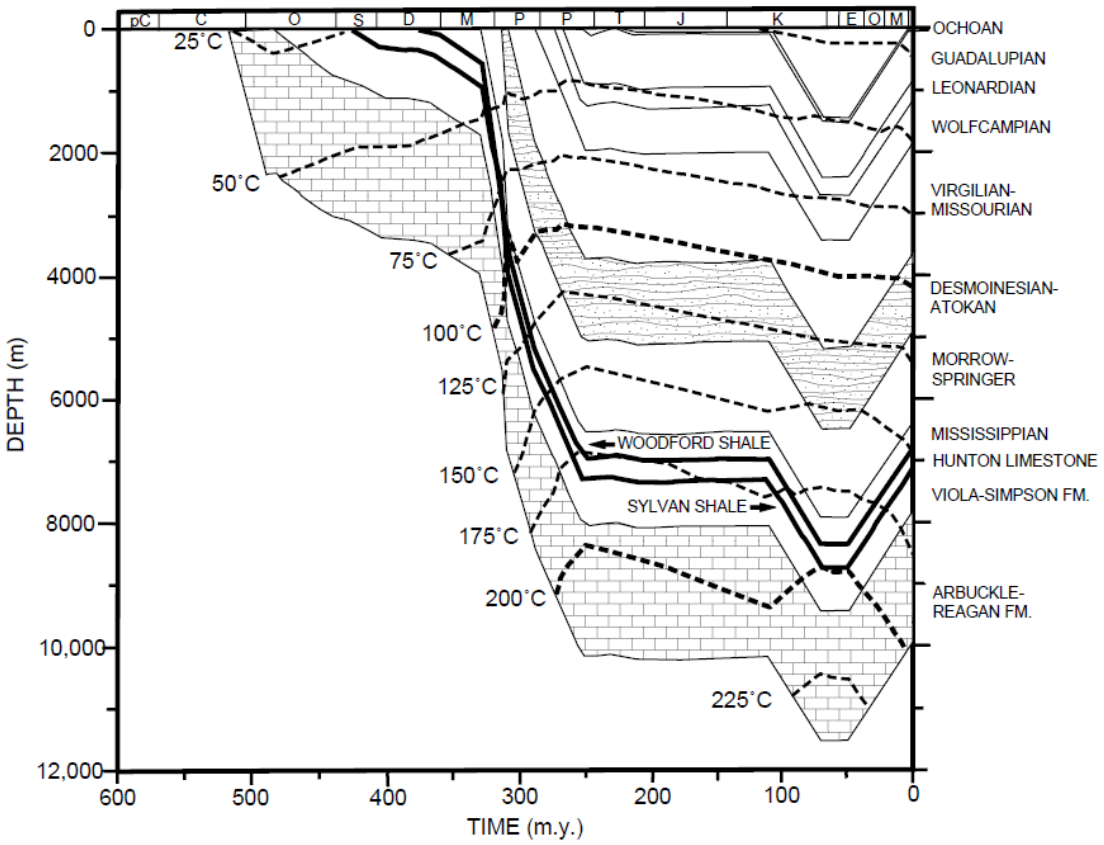

Figure 24: Basin model (modified from Carter et al., 1998) for the study area near the core provided for the paleomagnetic study.

therefore, sufficient thermal conditions were present to source a CRM originated by hydrocarbons. Presently, the paleomagnetism offers a critical temporal component on the petroleum system evolution, additional paleotemperature data would help to validate the CRM origin and basin understanding.

CONCLUSION

The Meramec and Osage deposits of the STACK and NW STACK in the Anadarko Basin record a number of auto and allo-cyclic controls on diagenesis; such as storms and sea level fluctuations, respectively. The unveiling of the diagenetic history and reservoir quality controls of the Meramec and Osage were evaluated through the novel integration of petrography, petrophysics, and paleomagnetism. The principal findings of the study are:

1. The Osage of the STACK and NW STACK contain authigenic fracture fill of mega-quartz, baroque dolomite, and calcite characteristic of hydrothermal fluid flow in the Anadarko Basin.
2. Meteoric diagenesis in the Osage enhanced porosity development in the form of moldic pores in leached sponge spicules and intercrystalline porosity in silicified matrix.
3. A strong correlation between sequence stratigraphy and diagenesis is observed in the Meramec. Flooding surfaces are often the upper bound of shallowing parasequences rich in skeletal fragments and high primary porosity, resulting in pervasive marine calcite cementation. Clay in more argillaceous microfacies partially protects primary porosity and can enhance later secondary dissolution.

4. The primary pore-types observed in the Meramec are dissolution pores in feldspars, interstitial pores in clay, and intergranular pores between framework grains. These pore-types are variably distributed across each microfacies. The interstitial clay associated porosity is most abundant in the argillaceous siltstone, and the dissolved pores are most abundant in the calcitic siltstone.
5. Log responses can be grouped in the Meramec to provide a framework for defining the mineralogical and reservoir property trends through the section. Hierarchal clustering analysis identified the intervals of greatest dissolution in the calcitic siltstone microfacies and confirmed the storage capacity of the argillaceous siltstone microfacies.
6. Paleomagnetic results illustrate a CRM held in magnetite that formed at approximately 300 Ma. The secondary remagnetization is interpreted to be a result of hydrocarbon emplacement; thereby, providing a temporal component in the diagenetic evolution of the Meramec and Osage deposits.

REFERENCES

AlBahadily, J. K. R., & Nasser, M. E. (2017). Role of the Cluster Analysis in Logfacies and Depositional Environments Recognition from Well Log Response for Mishrif Formation in Southeast Iraq.

Al-Ramadan, K., S. Morad, J. N. Proust, and I. S. Al-Aasm (2005) Distribution of diagenetic alterations in siliciclastic shoreface deposits within a sequence stratigraphic framework: Evidence from the Upper Jurassic, Boulonnais, NW France: Journal of Sedimentary Research, v. 75, p. 943–959, doi:10.2110/jsr.2005.072.

Ali, S. A., Clark, W. J., Moore, W. R., & Dribus, J. R. (2010). Diagenesis and reservoir quality. Oilfield Review, 22(2), 14-27.

Arason, Þ., & Levi, S. (2010). Maximum likelihood solution for inclination-only data in paleomagnetism. Geophysical Journal International, 182(2), 753-771.

Audunsson, H., & Levi, S. (1989). Drilling-induced remanent magnetization in basalt drill cores. Geophysical Journal International, 98(3), 613-622.

Bjorlykke, K., & Egeberg, P. K. (1993). Quartz cementation in sedimentary basins. AAPG bulletin, 77(9), 1538-1548.

Boyd, D. T. (2008). Stratigraphic guide to Oklahoma oil and gas reservoirs: Oklahoma Geological Society, Special Publication 2008-1, 2 p.

Braun, J. C. (1959). A Stratigraphic Study of the Sycamore and Related Formations in the Southeastern Anadarko Basin. Shale Shaker, September 1959, pp. 150-164.

Burmester, R. F. (1977). Origin and stability of drilling induced remanence. Geophysical Journal of the Royal Astronomical Society, 48(1), 1-14.

Cardott, B. J. (2014, May). Woodford shale play update: expanded extent in the oil window. In AAPG education directorate Woodford shale forum. American Association of Petroleum Geologists, Oklahoma City, OK, USA (Vol. 29).

Carter, L. S., Kelley, S. A., Blackwell, D. D., and Naeser, D. N. (1998). Heat flow and thermal history of the Anadarko Basin, Oklahoma, AAPG Bulletin, V. 82, No. 2, p. 291-316.

Carvalho, M. V. F., L. F. De Ros, and N. S. Gomes (1995). Carbonate cementation patterns and diagenetic reservoir facies in the Campos Basin Cretaceous turbidites, offshore eastern Brazil: Marine and Petroleum Geology, v. 12, p. 741–758, doi:10.1016/0264-8172(95)93599-Y.

Coffey, W. S. (2000) The diagenetic history and depositional system of the Sycamore Formation (Mississippian), Carter-Knox Field, Grady and Stephens Counties, Oklahoma: Doctorale dissertation, Oklahoma State University, Stillwater, Oklahoma. 167p.

Cullen, A. (2017). Devonian-Mississippian Petroleum Systems of Southern Laurasia: What Makes the STACK-Merge-SCOOP Play in Oklahoma so Special: Devonian-Mississippian Petroleum Systems of Southern Laurasia: What Makes the STACK-MERGE-SCOOP in Oklahoma so Special? AAPG Playmaker Forum Oklahoma City, OK 2017.

Culp, C. K. (1961). Stratigraphic relations of the Sycamore limestone (Mississippian) in southern Oklahoma: Oklahoma City Geological Society, The Shale Shaker Digest V, V. IX-XI, No. 3, p. 446- 457.

Dehcheshmehi, S. M. (2016). Regional Diagenesis of Mississippian Strata of the Southern Mid-Continent, USA (Doctoral dissertation, Oklahoma State University).

Ehrenberg, S. N., & Jakobsen, K. G. (2001). Plagioclase dissolution related to biodegradation of oil in Brent Group sandstones (Middle Jurassic) of Gullfaks Field, northern North Sea. Sedimentology, 48(4), 703-721.

Elmore, R. D., & Crawford, L. (1990). Remanence in authigenic magnetite: Testing the hydrocarbon-magnetite hypothesis. Journal of Geophysical Research: Solid Earth, 95(B4), 4539-4549.

Elmore, R. D., London, D., Bagley, D., Fruit, D., & Gao, G. (1993). Remagnetization by basinal fluids: testing the hypothesis in the Viola Limestone, southern Oklahoma. Journal of Geophysical Research: Solid Earth, 98(B4), 6237-6254.

Feinstein, S. (1981). Subsidence and thermal history of Southern Oklahoma Aulocogen: Implications for petroleum exploration, AAPG Bulletin, V. 65, No. 12, p. 2521-2533.

Fontana, D., E. F. McBride, and R. Kluger (1986). Diagenesis and porosity evolution of submarine-fan and basin-plain sandstones, Marnoso-Arenacea Formation, northern Apennines, Italy: Bulletin of Canadian Petroleum Geology, v. 34, p. 313–328.

Gilbert, M. C. (1983). Timing and chemistry of igneous events associated with the southern Oklahoma aulacogen. In Developments in Geotectonics (Vol. 19, pp. 439-455). Elsevier.

Goldstein, R., & King, B. (2014). History of hydrothermal fluid flow in the Midcontinent: A key to understanding the origin and distribution of porosity. In AAPG Mississippian Lime Forum, February (Vol. 20, p. 2014).

Ham, W. E., & Wilson, J. L. (1967). Paleozoic epeirogeny and orogeny in the central United States. American Journal of Science, 265(5), 332-407.

Harris, S. A. (1975). Hydrocarbon accumulation in "Meramec-Osage" (Mississippian) rocks, Sooner Trend, northwest-central Oklahoma: AAPG Bulletin, v. 59, p. 633–664.

Hayes J.B. (1979). Sandstone diagenesis-whole truth. In: Aspect of Diagenesis (ed. Scholle P.A. and Schluger P.R) Specs. Soc. Econ. Paleont. Miner. Tulsa,26, 127-140.

Hirt, A. M., Banin, A. & Gehring, U. A. (1993). Thermal generation of ferromagnetic minerals from iron enriched smectites. Geophysical Journal International, 115, 1161–1168.

James, W. C. (1992). Sandstone diagenesis inmixed siliciclastic carbonate sequences: Quadrant and Tensleep formations (Pennsylvanian), northern Rocky Mountains: Journal of Sedimentary Petrology, v. 62, p. 810–824.

Johnson, K. S., Amsden, T. W., Denison, R. E., Dutton, S. P., Goldstein, A. G., Rascoe, B., ... & Thompson, D. M. (1989). Geology of the southern Midcontinent. Oklahoma Geological Survey Special Publication, 89(2), 53.

Johnson, K.S., Cardott, B.J. (1992). Geologic Framework and Hydrocarbon Source Rocks of Oklahoma. In: Johnson, K.S., Cardott, B.J. (Eds.), Source Rocks in the Southern Midcontinent, 1990 Symposium: Oklahoma Geological Survey Circular, 93, pp. 21–37.

Katz, B., Elmore, R. D., Cogoini, M. & Ferry, S. (1998). Widespread chemical remagnetization: orogenic fluids or burial diagenesis of clays? Geology, 23, 603–606.

Keller, G. R., Lidiak, E. G., Hinze, W. J., & Braile, L. W. (1983). The role of rifting in the tectonic development of the midcontinent, USA. In Developments in Geotectonics (Vol. 19, pp. 391-412). Elsevier.

Keller, G.R. (2014). The southern Oklahoma aulacogen: It's a classic. In Suneson, N. (ed.), Igneous and Tectonic History of the Southern Oklahoma Aulacogen: Oklahoma Geological Survey Guidebook (Vol. 38, pp. 389-391).

Kennedy, M. J., Pevear, D. R. & Hill, R. J. (2002). Mineral surface control of organic carbon in black shale. Science, 295, 657– 660.

Kent, D.V. (1985). Thermoviscous remagnetization in some Appalachian limestones: Geophysical Research Letters, v. 12, p. 805–808, doi: 10.1029/GL012i012p00805.

Ketzer, J. M., S. Morad, R. Evans, and I. Al-Aasm (2002). Distribution of diagenetic alterations in fluvial, deltaic, and shallow marine sandstones within a sequence stratigraphic framework: Evidence from the Mullaghmore Formation (Carboniferous), NWIreland: Journal of Sedimentary Research, v. 72, p. 760–774, doi:10.1306/042202720760.

Ketzer, J. M., and S. Morad (2006). Predictive distribution of shallow marine, low-porosity (pseudomatrix -rich) sandstones in a sequence stratigraphic framework—Example from the Ferron Sandstone, Upper Cretaceous, U.S.A.: Maine and Petroleum Geologists, v. 23, p. 29–36, doi: 10.1016/j.marpetgeo.2005.05.001.

Kirschvink, J.L., (1980). The least-squares line and plane and the analysis of palaeomagnetic data. Geophysical Journal International, 62(3), pp.699-718.

Mansurbeg, H., M. A. Caja, R. M. Marfil, S., E. Remacha, D. Garcia, T. Martín-Crespo, M. A. K. El-Ghali, and J. P. Nystuen (2009). Diagenetic evolution and porosity destruction of turbiditic hybrid arenites and siliciclastic sandstones of foreland basins: Evidence from the Eocene Hecho Group, Pyrenees, Spain: Journal of Sedimentary Research, v. 79, p. 711–735, doi:10.2110/jsr.2009.060.

Mazzullo, S. J., Wilhite, B. W., & Woolsey, I. W. (2009). Petroleum reservoirs within a spiculite-dominated depositional sequence: Cowley Formation (Mississippian: Lower Carboniferous), south-central Kansas. AAPG bulletin, 93(12), 1649-1689.

Mikkelson, D. H. (1966). The origin and age of the Mississippian “chat” in north-central Oklahoma: Oklahoma City Geological Society, Shale Shaker Digest, v. 5, p. 255–265.

Miller, J. (2018). Regional stratigraphy and organic richness of the Mississippian Meramec and associated strata, Anadarko Basin, central Oklahoma: Master’s Thesis, University of Oklahoma.

Molenaar, N. (1990). Calcite cementation in shallow marine Eocene sandstones and constraints of early diagenesis. Journal of the Geological Society, 147(5), 759-768.

Morad, S., Al-Ramadan, K., Ketzer, J. M., & De Ros, L. F. (2010). The impact of diagenesis on the heterogeneity of sandstone reservoirs: A review of the role of depositional facies and sequence stratigraphy. AAPG bulletin, 94(8), 1267-1309.

Nedkvitne, T., Karlsen, D. A., Bjørlykke, K., & Larter, S. R. (1993). Relationship between reservoir diagenetic evolution and petroleum emplacement in the Ula Field, North Sea. Marine and Petroleum Geology, 10(3), 255-270.

Nicholas, R. L., & Rozendal, R. A. (1975). Subsurface positive elements within Ouachita foldbelt in Texas and their relation to Paleozoic cratonic margin. AAPG Bulletin, 59(2), 193-216.

Northcutt, R.A. and J.A. Campbell, (1998). Geologic Provinces of Oklahoma: Basement Tectonics, 12, 29-37.

Parham, K. D., and R. A. Northcutt (1993). MS-3, Mississippian chert and carbonate and basal Pennsylvanian sandstone—central Kansas uplift and northern Oklahoma, in D. G. Bebout, W. A. White, T. F. Hentz, and M. K. Grasmick, eds., Atlas of major mid-continent gas reservoirs: Gas Research Institute and Texas Bureau of Economic Geology, p. 57–60.

Pullaiah, G., Irving, E., Buchan, K.L., and Dunlop, D.J. (1975). Magnetization changes caused by burial and uplift: Earth and Planetary Science Letters, v. 28, p. 133-143, doi: 10.1016/0012-821X (75)90221-6.

Perry, W. J. (1989). Tectonic evolution of the Anadarko Basin region, Oklahoma (No. 1866). Department of the Interior, US Geological Survey.

Prestridge, J. D. (1957). A subsurface stratigraphic study of the Sycamore Formation in the Ardmore Basin (Doctoral dissertation, University of Oklahoma).

Price, B., K. Haustveit, and A. Lamb (2017). Influence of stratigraphy on barriers to fracture growth and completion optimization in the Meramec Stack Play, Anadarko Basin, Oklahoma: Unconventional Resources Technology Conference (URTEC), Article #2697585.

Puzin, L. A. (1951). A chart of connate water resistivity in Oklahoma and its application to electric log interpretation: Petroleum Engineering, v. 24, no. 9, p. B67-B78.

Roberts, J. (2017). A Diagenetic and Paleomagnetic Study of the Woodford Shale, Oklahoma, USA (Doctoral dissertation, University of Oklahoma).

Rogers, S. M. (1996). Depositional and diagenetic history of the Mississippian chat, north-central Oklahoma: Master's thesis, University of Oklahoma, Norman, Oklahoma.

Rogers, S. M. (2001). Deposition and diagenesis of Mississippian chat reservoirs, north-central Oklahoma: AAPG Bulletin, v. 85, no.1, p 115-129.

Schieber, J. (2011). Iron Sulfide Formation: Encyclopedia of Geobiology, 486-502, doi: 10.1007/978-1-4020-9212-1_118

Schwartzapfel, J. A. (1996). Upper Devonian and Mississippian radiolarian zonation and biostratigraphy of the Woodford, Sycamore, Caney and Goddard formations, Oklahoma. Cushman Foundation for Foraminiferal Research, Spec. Publ., 33, 1-275.

Stanley, S. M., Ries, J. B., & Hardie, L. A. (2002). Low-magnesium calcite produced by coralline algae in seawater of Late Cretaceous composition. Proceedings of the National Academy of Sciences, 99(24), 15323-15326.

Ulmer-Scholle, D. S., Scholle, P. A., Schieber, J., & Raine, R. J (2015). A Color Guide to the Petrography of Sandstones, Siltstones, Shales and Associated Rocks. Tulsa, OK: American Association of Petroleum Geologists.

Walderhaug, O. (2000). Modeling quartz cementation and porosity in Middle Jurassic Brent Group sandstones of the Kvitebjørn field, northern North Sea. AAPG bulletin, 84(9), 1325-1339.

Watney, W. L., Guy, W. J., & Byrnes, A. P. (2001). Characterization of the Mississippian chat in south-central Kansas. AAPG bulletin, 85(1), 85-113.

Welch, S. A., & Ullman, W. J. (1996). Feldspar dissolution in acidic and organic solutions: Compositional and pH dependence of dissolution rate. Geochimica et Cosmochimica Acta, 60(16), 2939-2948.

Wethington, N. (2017). Stratigraphic Architecture of the Mississippian Limestone Through Integrated Electrofacies Classification, Hardtner Field Area, Kansas and Oklahoma: Master's thesis, University of Oklahoma, Norman, Oklahoma. 1 p.

Wickham, J. S. (1978). The southern Oklahoma aulacogen, Geological Society of America, In structural style of the Arbuckle region, South-Central section Guidebook for field trip 3, p. 9-41.

Woods, S., Elmore, R. D. & Engel, M. (2002). Paleomagnetic dating of the smectite-to-illite conversion: testing the hypothesis in Jurassic sedimentary rocks, Skye, Scotland. Journal of Geophysical Research, 107, 2091, http://dx.doi.org/10.1029/2000JB000053

Zijderveld, J.D.A. (1967). A.C. demagnetization of rocks: Analysis of results. In: Collinson, D. E., Creer, K. M. & Runcorn , S. K. (eds) 1967. Methods in Paleomagnetism, 254-286.